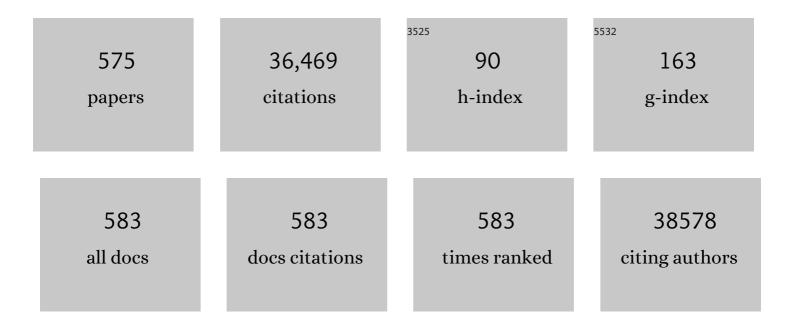
List of Publications by Year in descending order

Source: https://exaly.com/author-pdf/4363988/publications.pdf Version: 2024-02-01



Howeluu

#	Article	IF	CITATIONS
1	Applications of 2D MXenes in energy conversion and storage systems. Chemical Society Reviews, 2019, 48, 72-133.	18.7	1,354
2	Synthesis of Few‣ayer MoS <sub>2</sub> Nanosheet oated TiO <sub>2</sub> Nanobelt Heterostructures for Enhanced Photocatalytic Activities. Small, 2013, 9, 140-147.	5.2	1,166
3	Ni3S2 nanorods/Ni foam composite electrode with low overpotential for electrocatalytic oxygen evolution. Energy and Environmental Science, 2013, 6, 2921.	15.6	939
4	Self-Assembled Copper–Amino Acid Nanoparticles for in Situ Glutathione "AND― H <sub>2</sub> O <sub>2</sub> Sequentially Triggered Chemodynamic Therapy. Journal of the American Chemical Society, 2019, 141, 849-857.	6.6	850
5	Recent progress in design, synthesis, and applications of one-dimensional TiO <sub>2</sub> nanostructured surface heterostructures: a review. Chemical Society Reviews, 2014, 43, 6920-6937.	18.7	726
6	One-step synthesis of Ni <sub>3</sub> S <sub>2</sub> nanorod@Ni(OH) <sub>2</sub> nanosheet core–shell nanostructures on a three-dimensional graphene network for high-performance supercapacitors. Energy and Environmental Science, 2013, 6, 2216-2221.	15.6	554
7	Hierarchical porous carbon aerogel derived from bagasse for high performance supercapacitor electrode. Nanoscale, 2014, 6, 12120-12129.	2.8	545
8	Graphene-based nitrogen self-doped hierarchical porous carbon aerogels derived from chitosan for high performance supercapacitors. Nano Energy, 2015, 15, 9-23.	8.2	531
9	A Bi <sub>2</sub> WO <sub>6</sub> â€Based Hybrid Photocatalyst with Broad Spectrum Photocatalytic Properties under UV, Visible, and Nearâ€Infrared Irradiation. Advanced Materials, 2013, 25, 5075-5080.	11.1	530
10	From UV to Nearâ€Infrared, WS <sub>2</sub> Nanosheet: A Novel Photocatalyst for Full Solar Light Spectrum Photodegradation. Advanced Materials, 2015, 27, 363-369.	11.1	494
11	Ag <sub>2</sub> 0/TiO <sub>2</sub> Nanobelts Heterostructure with Enhanced Ultraviolet and Visible Photocatalytic Activity. ACS Applied Materials & Interfaces, 2010, 2, 2385-2392.	4.0	489
12	Dynamic Pressure Mapping of Personalized Handwriting by a Flexible Sensor Matrix Based on the Mechanoluminescence Process. Advanced Materials, 2015, 27, 2324-2331.	11.1	468
13	Enhanced Ferroelectric-Nanocrystal-Based Hybrid Photocatalysis by Ultrasonic-Wave-Generated Piezophototronic Effect. Nano Letters, 2015, 15, 2372-2379.	4.5	428
14	Carbon quantum dots/hydrogenated TiO2 nanobelt heterostructures and their broad spectrum photocatalytic properties under UV, visible, and near-infrared irradiation. Nano Energy, 2015, 11, 419-427.	8.2	416
15	Synthesis of CuO nanostructures and their application for nonenzymatic glucose sensing. Sensors and Actuators B: Chemical, 2010, 144, 220-225.	4.0	375
16	Ultrathin N-Doped Mo <sub>2</sub> C Nanosheets with Exposed Active Sites as Efficient Electrocatalyst for Hydrogen Evolution Reactions. ACS Nano, 2017, 11, 12509-12518.	7.3	350
17	Metal Halide Perovskite Nanosheet for X-ray High-Resolution Scintillation Imaging Screens. ACS Nano, 2019, 13, 2520-2525.	7.3	346
18	3D Bi <sub>2</sub> MoO <sub>6</sub> Nanosheet/TiO <sub>2</sub> Nanobelt Heterostructure: Enhanced Photocatalytic Activities and Photoelectochemistry Performance. ACS Catalysis, 2015, 5, 4530-4536.	5.5	323

#	Article	IF	CITATIONS
19	Water Splitting: From Electrode to Green Energy System. Nano-Micro Letters, 2020, 12, 131.	14.4	288
20	Structure, Synthesis, and Applications of TiO <sub>2</sub> Nanobelts. Advanced Materials, 2015, 27, 2557-2582.	11.1	287
21	La(OH)3 and La2O3 Nanobelts—Synthesis and Physical Properties. Advanced Materials, 2007, 19, 470-474.	11.1	277
22	Enhanced Photocatalytic Performances of CeO <sub>2</sub> /TiO <sub>2</sub> Nanobelt Heterostructures. Small, 2013, 9, 3864-3872.	5.2	262
23	MoO2 nanobelts@nitrogen self-doped MoS2 nanosheets as effective electrocatalysts for hydrogen evolution reaction. Journal of Materials Chemistry A, 2014, 2, 11358.	5.2	262
24	Self-Powered Electrical Stimulation for Enhancing Neural Differentiation of Mesenchymal Stem Cells on Graphene–Poly(3,4-ethylenedioxythiophene) Hybrid Microfibers. ACS Nano, 2016, 10, 5086-5095.	7.3	249
25	Flexible Electronics Based on Micro/Nanostructured Paper. Advanced Materials, 2018, 30, e1801588.	11.1	249
26	Silver nanoparticle-decorated porous ceramic composite for water treatment. Journal of Membrane Science, 2009, 331, 50-56.	4.1	247
27	Nanostructured Sheets of TiO Nanobelts for Gas Sensing and Antibacterial Applications. Advanced Functional Materials, 2008, 18, 1131-1137.	7.8	245
28	Enhanced catalytic performance by multi-field coupling in KNbO3 nanostructures: Piezo-photocatalytic and ferro-photoelectrochemical effects. Nano Energy, 2019, 58, 695-705.	8.2	240
29	A Photoresponsive Rutile TiO <sub>2</sub> Heterojunction with Enhanced Electron–Hole Separation for Highâ€Performance Hydrogen Evolution. Advanced Materials, 2019, 31, e1806596.	11.1	240
30	Three-Dimensional Hierarchical Frameworks Based on MoS <sub>2</sub> Nanosheets Self-Assembled on Graphene Oxide for Efficient Electrocatalytic Hydrogen Evolution. ACS Applied Materials & Interfaces, 2014, 6, 21534-21540.	4.0	235
31	Engineering the Absorption and Field Enhancement Properties of Au–TiO <sub>2</sub> Nanohybrids <i>via</i> Whispering Gallery Mode Resonances for Photocatalytic Water Splitting. ACS Nano, 2016, 10, 4496-4503.	7.3	230
32	Paper-Based Electrochemical Sensing Platform with Integral Battery and Electrochromic Read-Out. Analytical Chemistry, 2012, 84, 2528-2532.	3.2	219
33	Fullâ€Spectrum Solarâ€Lightâ€Activated Photocatalysts for Light–Chemical Energy Conversion. Advanced Energy Materials, 2017, 7, 1700473.	10.2	213
34	One-dimensional single-crystalline Ti–O based nanostructures: properties, synthesis, modifications and applications. Journal of Materials Chemistry, 2010, 20, 5993.	6.7	195
35	Composite-Hydroxide-Mediated Approach for the Synthesis of Nanostructures of Complex Functional-Oxides. Nano Letters, 2006, 6, 1535-1540.	4.5	194
36	Heterostructures construction on TiO2 nanobelts: A powerful tool for building high-performance photocatalysts. Applied Catalysis B: Environmental, 2017, 202, 620-641.	10.8	194

#	Article	IF	CITATIONS
37	Ultrathin MoO 3 nanocrystalsself-assembled on graphene nanosheets via oxygen bonding as supercapacitor electrodes of high capacitance and long cycle life. Nano Energy, 2015, 12, 510-520.	8.2	192
38	One-step synthesis of CdS nanoparticles/MoS 2 nanosheets heterostructure on porous molybdenum sheet for enhanced photocatalytic H 2 evolution. Applied Catalysis B: Environmental, 2017, 210, 290-296.	10.8	192
39	Enhancement of Ethanol Vapor Sensing of TiO <sub>2</sub> Nanobelts by Surface Engineering. ACS Applied Materials & Interfaces, 2010, 2, 3263-3269.	4.0	188
40	Development of Conductive Hydrogels for Fabricating Flexible Strain Sensors. Small, 2022, 18, e2101518.	5.2	188
41	Enhancing the electrochemical performance of lithium ion batteries using mesoporous Li3V2(PO4)3/C microspheres. Journal of Materials Chemistry, 2012, 22, 5960.	6.7	176
42	Sol–gel preparation of transparent zinc oxide films with highly preferential crystal orientation. Vacuum, 2004, 77, 57-62.	1.6	173
43	Highly Morphology ontrollable and Highly Sensitive Capacitive Tactile Sensor Based on Epidermisâ€Dermisâ€Inspired Interlocked Asymmetricâ€Nanocone Arrays for Detection of Tiny Pressure. Small, 2020, 16, e1904774.	5.2	166
44	Structure, Conductivity, and Thermopower of Crystalline Polyaniline Synthesized by the Ultrasonic Irradiation Polymerization Method. Macromolecules, 2002, 35, 9414-9419.	2.2	165
45	Sulfur and nitrogen self-doped carbon nanosheets derived from peanut root nodules as high-efficiency non-metal electrocatalyst for hydrogen evolution reaction. Nano Energy, 2015, 16, 357-366.	8.2	162
46	Direct synthesis and structure characterization of ultrafine CeO2nanoparticles. Nanotechnology, 2006, 17, 5983-5987.	1.3	159
47	Photocatalysis from UV/Vis to Nearâ€Infrared Light: Towards Full Solarâ€Light Spectrum Activity. ChemCatChem, 2015, 7, 559-573.	1.8	148
48	Confined distribution of platinum clusters on MoO2 hexagonal nanosheets with oxygen vacancies as a high-efficiency electrocatalyst for hydrogen evolution reaction. Nano Energy, 2019, 62, 127-135.	8.2	143
49	Nanoheterostructures on TiO2 nanobelts achieved by acid hydrothermal method with enhanced photocatalytic and gas sensitive performance. Journal of Materials Chemistry, 2011, 21, 7937.	6.7	142
50	Metallic Ni3Mo3N Porous Microrods with Abundant Catalytic Sites as Efficient Electrocatalyst for Large Current Density and Superstability of Hydrogen Evolution Reaction and Water Splitting. Applied Catalysis B: Environmental, 2020, 272, 118956.	10.8	138
51	NiO–TiO2 p–n heterostructured nanocables bridged by zero-bandgap rGO for highly efficient photocatalytic water splitting. Nano Energy, 2015, 16, 207-217.	8.2	136
52	Gold and gold–palladium alloy nanoparticles on heterostructured TiO <sub>2</sub> nanobelts as plasmonic photocatalysts for benzyl alcohol oxidation. Nanoscale, 2015, 7, 209-217.	2.8	136
53	In2S3 nanomaterial as a broadband spectrum photocatalyst to display significant activity. Applied Catalysis B: Environmental, 2015, 176-177, 83-90.	10.8	135
54	Few-layered MoS <sub>2</sub> nanosheets wrapped ultrafine TiO <sub>2</sub> nanobelts with enhanced photocatalytic property. Nanoscale, 2016, 8, 6101-6109.	2.8	131

#	Article	IF	CITATIONS
55	Enhanced Photocatalytic Property of Reduced Graphene Oxide/TiO <sub>2</sub> Nanobelt Surface Heterostructures Constructed by an In Situ Photochemical Reduction Method. Small, 2014, 10, 3775-3782.	5.2	130
56	Ni@NiO Nanowires on Nickel Foam Prepared via "Acid Hungry―Strategy: High Supercapacitor Performance and Robust Electrocatalysts for Water Splitting Reaction. Small, 2018, 14, e1800294.	5.2	130
57	Regulating the vertical phase distribution by fullerene-derivative in high performance ternary organic solar cells. Nano Energy, 2018, 46, 81-90.	8.2	129
58	Photoluminescence Origin of Zero-Dimensional Cs <sub>4</sub> PbBr <sub>6</sub> Perovskite. ACS Energy Letters, 2020, 5, 87-99.	8.8	128
59	Construction of a 3D rGO–collagen hybrid scaffold for enhancement of the neural differentiation of mesenchymal stem cells. Nanoscale, 2016, 8, 1897-1904.	2.8	127
60	Surface modification and functionalization of silk fibroin fibers/fabric toward high performance applications. Materials Science and Engineering C, 2012, 32, 627-636.	3.8	126
61	Promotion of Overall Water Splitting Activity Over a Wide pH Range by Interfacial Electrical Effects of Metallic NiCoâ€nitrides Nanoparticle/NiCo <sub>2</sub> O <sub>4</sub> Nanoflake/graphite Fibers. Advanced Science, 2019, 6, 1801829.	5.6	122
62	Ultrasensitive Physical, Bio, and Chemical Sensors Derived from 1â€, 2â€, and 3â€Ð Nanocellulosic Materials. Small, 2020, 16, e1906567.	5.2	122
63	Chemical assembly of TiO2 and TiO2@Ag nanoparticles on silk fiber to produce multifunctional fabrics. Journal of Colloid and Interface Science, 2011, 358, 307-315.	5.0	120
64	WSe <sub>2</sub> 2D pâ€type semiconductorâ€based electronic devices for information technology: Design, preparation, and applications. InformaÄnÃ-Materiály, 2020, 2, 656-697.	8.5	115
65	Nano-p–n junctions on surface-coarsened TiO2 nanobelts with enhanced photocatalytic activity. Journal of Materials Chemistry, 2011, 21, 5106.	6.7	114
66	Multifunctional Carbon–Silica Nanocapsules with Gold Core for Synergistic Photothermal and Chemo ancer Therapy under the Guidance of Bimodal Imaging. Advanced Functional Materials, 2016, 26, 4252-4261.	7.8	113
67	Tunable Layered (Na,Mn)V <sub>8</sub> O <sub>20</sub> · <i>n</i> H <sub>2</sub> O Cathode Material for Highâ€Performance Aqueous Zinc Ion Batteries. Advanced Science, 2020, 7, 2000083.	5.6	113
68	Ru–Ru <sub>2</sub> PΦNPC and NPC@RuO <sub>2</sub> Synthesized via Environmentâ€Friendly and Solidâ€Phase Phosphating Process by Saccharomycetes as N/P Sources and Carbon Template for Overall Water Splitting in Acid Electrolyte. Advanced Functional Materials, 2019, 29, 1901154.	7.8	112
69	High-Performance Symmetric Supercapacitor Constructed Using Carbon Cloth Boosted by Engineering Oxygen-Containing Functional Groups. ACS Applied Materials & Interfaces, 2019, 11, 18044-18050.	4.0	110
70	Synthesis of scaly Sn <sub>3</sub> O <sub>4</sub> /TiO <sub>2</sub> nanobelt heterostructures for enhanced UV-visible light photocatalytic activity. Nanoscale, 2015, 7, 3117-3125.	2.8	108
71	TiO <sub>2</sub> @Carbon Photocatalysts: The Effect of Carbon Thickness on Catalysis. ACS Applied Materials & Interfaces, 2016, 8, 1903-1912.	4.0	108
72	Phase transformation of TiO2 nanobelts and TiO2(B)/anatase interface heterostructure nanobelts with enhanced photocatalytic activity. CrystEngComm, 2011, 13, 6643.	1.3	107

#	Article	IF	CITATIONS
73	Hierarchical TiO2 nanowire/graphite fiber photoelectrocatalysis setup powered by a wind-driven nanogenerator: A highly efficient photoelectrocatalytic device entirely based on renewable energy. Nano Energy, 2015, 11, 19-27.	8.2	107
74	Oneâ€Đimensional Ferroelectric Nanostructures: Synthesis, Properties, and Applications. Advanced Science, 2016, 3, 1500358.	5.6	107
75	Ni-Co-N hybrid porous nanosheets on graphene paper for flexible and editable asymmetric all-solid-state supercapacitors. Nano Energy, 2019, 61, 18-26.	8.2	107
76	Zinc oxide films prepared by sol–gel method. Journal of Crystal Growth, 2005, 275, e943-e946.	0.7	104
77	Effects of Graphene Quantum Dots on the Selfâ€Renewal and Differentiation of Mesenchymal Stem Cells. Advanced Healthcare Materials, 2016, 5, 702-710.	3.9	103
78	Molybdenum carbide on hierarchical porous carbon synthesized from Cu-MoO2 as efficient electrocatalysts for electrochemical hydrogen generation. Nano Energy, 2017, 41, 749-757.	8.2	103
79	Synthesis of Bi2Se3 thermoelectric nanosheets and nanotubes through hydrothermal co-reduction method. Journal of Solid State Chemistry, 2004, 177, 4001-4006.	1.4	102
80	Cobalt–Cobalt Phosphide Nanoparticles@Nitrogenâ€Phosphorus Doped Carbon/Graphene Derived from Cobalt Ions Adsorbed <i>Saccharomycete</i> Yeasts as an Efficient, Stable, and Largeâ€Currentâ€Density Electrode for Hydrogen Evolution Reactions. Advanced Functional Materials, 2018, 28, 1801332.	7.8	102
81	Encapsulation of a Phaseâ€Change Material in Nanocapsules with a Wellâ€Defined Hole in the Wall for the Controlled Release of Drugs. Angewandte Chemie - International Edition, 2019, 58, 10606-10611.	7.2	102
82	Oxygen-incorporated MoX (X: S, Se or P) nanosheets via universal and controlled electrochemical anodic activation for enhanced hydrogen evolution activity. Nano Energy, 2019, 62, 338-347.	8.2	102
83	1D Ni–Co oxide and sulfide nanoarray/carbon aerogel hybrid nanostructures for asymmetric supercapacitors with high energy density and excellent cycling stability. Nanoscale, 2016, 8, 16292-16301.	2.8	101
84	Suppressing Photoinduced Charge Recombination via the Lorentz Force in a Photocatalytic System. Advanced Science, 2019, 6, 1901244.	5.6	101
85	Engineered Microstructure Derived Hierarchical Deformation of Flexible Pressure Sensor Induces a Supersensitive Piezoresistive Property in Broad Pressure Range. Advanced Science, 2020, 7, 2000154.	5.6	100
86	The hybrid nanostructure of MnCo <sub>2</sub> O <sub>4.5</sub> nanoneedle/carbon aerogel for symmetric supercapacitors with high energy density. Nanoscale, 2015, 7, 14401-14412.	2.8	99
87	Hierarchical microsphere of MoNi porous nanosheets as electrocatalyst and cocatalyst for hydrogen evolution reaction. Applied Catalysis B: Environmental, 2019, 249, 98-105.	10.8	98
88	Biopolymer/Calcium Phosphate Scaffolds for Bone Tissue Engineering. Advanced Healthcare Materials, 2014, 3, 469-484.	3.9	97
89	Microenvironment-Driven Bioelimination of Magnetoplasmonic Nanoassemblies and Their Multimodal Imaging-Guided Tumor Photothermal Therapy. ACS Nano, 2016, 10, 7094-7105.	7.3	97
90	Graphene Nanostructure-Based Tactile Sensors for Electronic Skin Applications. Nano-Micro Letters, 2019, 11, 71.	14.4	97

#	Article	IF	CITATIONS
91	Metallic Intermediate Phase Inducing Morphological Transformation in Thermal Nitridation: Ni <sub>3</sub> FeN-Based Three-Dimensional Hierarchical Electrocatalyst for Water Splitting. ACS Applied Materials & Interfaces, 2018, 10, 3699-3706.	4.0	96
92	Iron oxide embedded titania nanowires – An active and stable electrocatalyst for oxygen evolution in acidic media. Nano Energy, 2018, 45, 118-126.	8.2	95
93	Lignosulphonate-cellulose derived porous activated carbon for supercapacitor electrode. Journal of Materials Chemistry A, 2015, 3, 15049-15056.	5.2	93
94	YAC:Ce nano-sized phosphor particles prepared by a solvothermal method. Materials Research Bulletin, 2004, 39, 1923-1930.	2.7	92
95	Enhanced Performance of Layered Titanate Nanowire-Based Supercapacitor Electrodes by Nickel Ion Exchange. ACS Applied Materials & Interfaces, 2014, 6, 4578-4586.	4.0	92
96	Polylactic Acid Nanopillar Array-Driven Osteogenic Differentiation of Human Adipose-Derived Stem Cells Determined by Pillar Diameter. Nano Letters, 2018, 18, 2243-2253.	4.5	92
97	An Ultrarobust and Highâ€Performance Rotational Hydrodynamic Triboelectric Nanogenerator Enabled by Automatic Mode Switching and Charge Excitation. Advanced Materials, 2022, 34, e2105882.	11.1	92
98	Flexible wire-like all-carbon supercapacitors based on porous core–shell carbon fibers. Journal of Materials Chemistry A, 2014, 2, 7250-7255.	5.2	91
99	Hydrogenated TiO2 nanobelts as highly efficient photocatalytic organic dye degradation and hydrogen evolution photocatalyst. Journal of Hazardous Materials, 2015, 299, 165-173.	6.5	89
100	Microstructure and domain engineering of lithium niobate crystal films for integrated photonic applications. Light: Science and Applications, 2020, 9, 197.	7.7	89
101	Nonoxidized MXene Quantum Dots Prepared by Microexplosion Method for Cancer Catalytic Therapy. Advanced Functional Materials, 2020, 30, 2000308.	7.8	87
102	Microwave-assisted hydrothermal synthesis of Sn3O4 nanosheet/rGO planar heterostructure for efficient photocatalytic hydrogen generation. Applied Catalysis B: Environmental, 2018, 227, 470-476.	10.8	86
103	Photosensitization of TiO2 nanorods with CdS quantum dots for photovoltaic applications: A wet-chemical approach. Nano Energy, 2012, 1, 440-447.	8.2	85
104	Preparation of cellulose fiber–TiO2 nanobelt–silver nanoparticle hierarchically structured hybrid paper and its photocatalytic and antibacterial properties. Chemical Engineering Journal, 2013, 228, 272-280.	6.6	85
105	Conversion of solar power to chemical energy based on carbon nanoparticle modified photo-thermoelectric generator and electrochemical water splitting system. Nano Energy, 2018, 48, 481-488.	8.2	85
106	Tailoring the ruthenium reactive sites on N doped molybdenum carbide nanosheets via the anti-Ostwald ripening as efficient electrocatalyst for hydrogen evolution reaction in alkaline media. Applied Catalysis B: Environmental, 2020, 277, 119236.	10.8	85
107	Bone repair by periodontal ligament stem cell-seeded nanohydroxyapatite-chitosan scaffold. International Journal of Nanomedicine, 2012, 7, 5405.	3.3	83
108	Realization of Low Latent Heat of a Solar Evaporator via Regulating the Water State in Wood Channels. ACS Applied Materials & Interfaces, 2020, 12, 18504-18511.	4.0	83

#	Article	IF	CITATIONS
109	Ni-Ni3P nanoparticles embedded into N, P-doped carbon on 3D graphene frameworks via in situ phosphatization of saccharomycetes with multifunctional electrodes for electrocatalytic hydrogen production and anodic degradation. Applied Catalysis B: Environmental, 2020, 261, 118147.	10.8	82
110	Core–shell structured Fe3O4/PANI microspheres and their Cr(VI) ion removal properties. Synthetic Metals, 2013, 171, 1-6.	2.1	80
111	Fluorescent graphene quantum dots as traceable, pH-sensitive drug delivery systems. International Journal of Nanomedicine, 2015, 10, 6709.	3.3	79
112	Surface Charge Regulation of Osteogenic Differentiation of Mesenchymal Stem Cell on Polarized Ferroelectric Crystal Substrate. Advanced Healthcare Materials, 2015, 4, 998-1003.	3.9	79
113	In Vivo Tumor Visualization through MRI Offâ€On Switching of NaGdF <sub>4</sub> –CaCO <sub>3</sub> Nanoconjugates. Advanced Materials, 2019, 31, e1901851.	11.1	79
114	A three-dimensional multilevel nanoporous NiCoO <sub>2</sub> /Ni hybrid for highly reversible electrochemical energy storage. Journal of Materials Chemistry A, 2019, 7, 16222-16230.	5.2	77
115	Charge Redistribution Caused by S,P Synergistically Active Ru Endows an Ultrahigh Hydrogen Evolution Activity of Sâ€Doped RuP Embedded in N,P,Sâ€Doped Carbon. Advanced Science, 2020, 7, 2001526.	5.6	77
116	Preparation of highly dispersed YAG nano-sized powder by co-precipitation method. Materials Letters, 2006, 60, 962-965.	1.3	76
117	Composite-hydroxide-mediated approach as a general methodology for synthesizing nanostructures. Journal of Materials Chemistry, 2009, 19, 858.	6.7	75
118	Synthesis of monodisperse and spherical YAG nanopowder by a mixed solvothermal method. Journal of Alloys and Compounds, 2004, 372, 300-303.	2.8	74
119	A 2,7-carbazole-based dicationic salt for fluorescence detection of nucleic acids and two-photon fluorescence imaging of RNA in nucleoli and cytoplasm. Organic and Biomolecular Chemistry, 2011, 9, 3615.	1.5	74
120	BaTiO3 nanocrystal-mediated micro pseudo-electrochemical cells with ultrasound-driven piezotronic enhancement for polymerization. Nano Energy, 2017, 39, 461-469.	8.2	74
121	<i>In Vitro</i> Assessment of the Differentiation Potential of Bone Marrow-Derived Mesenchymal Stem Cells on Genipin-Chitosan Conjugation Scaffold with Surface Hydroxyapatite Nanostructure for Bone Tissue Engineering. Tissue Engineering - Part A, 2011, 17, 1341-1349.	1.6	73
122	Electrochemical Flocculation Integrated Hydrogen Evolution Reaction of Fe@Nâ€Doped Carbon Nanotubes on Iron Foam for Ultralow Voltage Electrolysis in Neutral Media. Advanced Science, 2019, 6, 1901458.	5.6	73
123	1319 nm and 1338 nm dual-wavelength operation of LD end-pumped Nd:YAG ceramic laser. Optics Express, 2010, 18, 9098.	1.7	72
124	High-Energy Faceted SnO <sub>2</sub> -Coated TiO <sub>2</sub> Nanobelt Heterostructure for Near-Ambient Temperature-Responsive Ethanol Sensor. ACS Applied Materials & Interfaces, 2015, 7, 24950-24956.	4.0	72
125	Cr(vi), Pb(ii), Cd(ii) adsorption properties of nanostructured BiOBr microspheres and their application in a continuous filtering removal device for heavy metal ions. Journal of Materials Chemistry A, 2014, 2, 2599.	5.2	71
126	Hydroxyapatite nanobelt/polylactic acid Janus membrane with osteoinduction/barrier dual functions for precise bone defect repair. Acta Biomaterialia, 2018, 71, 108-117.	4.1	71

#	Article	IF	CITATIONS
127	Band structure engineering of bioinspired Fe doped SrMoO4 for enhanced photocatalytic nitrogen reduction performance. Nano Energy, 2019, 66, 104187.	8.2	71
128	Hierarchical hybrid nanostructures of Sn <sub>3</sub> O <sub>4</sub> on N doped TiO <sub>2</sub> nanotubes with enhanced photocatalytic performance. Journal of Materials Chemistry A, 2015, 3, 19129-19136.	5.2	70
129	High yield production of reduced TiO2 with enhanced photocatalytic activity. Applied Surface Science, 2016, 360, 738-743.	3.1	70
130	Partial Nitridationâ€Induced Electrochemistry Enhancement of Ternary Oxide Nanosheets for Fiber Energy Storage Device. Advanced Energy Materials, 2018, 8, 1800685.	10.2	70
131	A simple gas sensor based on zinc ferrite hollow spheres: Highly sensitivity, excellent selectivity and long-term stability. Sensors and Actuators B: Chemical, 2019, 280, 34-40.	4.0	70
132	Microâ€∤Nanostructured Interface for Liquid Manipulation and Its Applications. Small, 2020, 16, e1903849.	5.2	70
133	Potential of MXene-Based Heterostructures for Energy Conversion and Storage. ACS Energy Letters, 2022, 7, 78-96.	8.8	69
134	Fabricating high-energy quantum dots in ultra-thin LiFePO <sub>4</sub> nanosheets using a multifunctional high-energy biomolecule—ATP. Energy and Environmental Science, 2014, 7, 2285-2294.	15.6	68
135	Energy-efficient, fully flexible, high-performance tactile sensor based on piezotronic effect: Piezoelectric signal amplified with organic field-effect transistors. Nano Energy, 2020, 76, 105050.	8.2	68
136	Manipulation of charge transfer in vertically aligned epitaxial ferroelectric KNbO3 nanowire array photoelectrodes. Nano Energy, 2017, 35, 92-100.	8.2	67
137	Graphene microfiber as a scaffold for regulation of neural stem cells differentiation. Scientific Reports, 2017, 7, 5678.	1.6	67
138	Rutile Nanorod/Anatase Nanowire Junction Array as Both Sensor and Power Supplier for Highâ€Performance, Selfâ€Powered, Wireless UV Photodetector. Small, 2016, 12, 2759-2767.	5.2	66
139	Structure-dependent electrode properties of hollow carbon micro-fibers derived from Platanus fruit and willow catkins for high-performance supercapacitors. Journal of Materials Chemistry A, 2017, 5, 2580-2591.	5.2	66
140	Designing a bioinspired synthetic tree by unidirectional freezing for simultaneous solar steam generation and salt collection. EcoMat, 2020, 2, e12018.	6.8	65
141	Graphene oxide-reinforced biodegradable genipin-cross-linked chitosan fluorescent biocomposite film and its cytocompatibility. International Journal of Nanomedicine, 2013, 8, 3415.	3.3	64
142	Hierarchical porous carbon with ordered straight micro-channels templated by continuous filament glass fiber arrays for high performance supercapacitors. Journal of Materials Chemistry A, 2017, 5, 1516-1525.	5.2	62
143	Synthesis of Monodispersed Spherical Yttrium Aluminum Garnet ( <scp>YAG</scp> ) Powders by a Homogeneous Precipitation Method. Journal of the American Ceramic Society, 2012, 95, 3821-3826.	1.9	61
144	PdO/TiO <sub>2</sub> and Pd/TiO <sub>2</sub> Heterostructured Nanobelts with Enhanced Photocatalytic Activity. Chemistry - an Asian Journal, 2014, 9, 1648-1654.	1.7	61

#	Article	IF	CITATIONS
145	Enhanced gas sensing property of SnO2 nanoparticles by constructing the SnO2–TiO2 nanobelt heterostructure. Journal of Alloys and Compounds, 2015, 639, 571-576.	2.8	61
146	Morphology and electronic structure modulation induced by fluorine doping in nickel-based heterostructures for robust bifunctional electrocatalysis. Nanoscale, 2018, 10, 20384-20392.	2.8	61
147	Calcium ion pinned vanadium oxide cathode for high-capacity and long-life aqueous rechargeable zinc-ion batteries. Science China Chemistry, 2020, 63, 1767-1776.	4.2	61
148	Multi-interface collaboration of graphene cross-linked NiS-NiS2-Ni3S4 polymorph foam towards robust hydrogen evolution in alkaline electrolyte. Nano Research, 2021, 14, 4857-4864.	5.8	61
149	Applications of 2D-Layered Palladium Diselenide and Its van der Waals Heterostructures in Electronics and Optoelectronics. Nano-Micro Letters, 2021, 13, 143.	14.4	61
150	Carbon-nanosphere-supported Pt nanoparticles for methanol and ethanol electro-oxidation in alkaline media. Journal of Power Sources, 2011, 196, 1904-1908.	4.0	60
151	Oxygen vacancies and Nâ€doping in organic–inorganic preâ€intercalated vanadium oxide for highâ€performance aqueous zincâ€ion batteries. InformaÀnÃ-Materiály, 2022, 4, .	8.5	60
152	Preparation and properties of YAG nano-sized powder from different precipitating agent. Optical Materials, 2004, 25, 407-412.	1.7	59
153	Pt nanoparticles supported on submicrometer-sized TiO2 spheres for effective methanol and ethanol oxidation. Electrochimica Acta, 2013, 105, 130-136.	2.6	59
154	Efficient photo-electrochemical water splitting based on hematite nanorods doped with phosphorus. Applied Catalysis B: Environmental, 2019, 248, 388-393.	10.8	59
155	Ultrasensitive Label-free MiRNA Sensing Based on a Flexible Graphene Field-Effect Transistor without Functionalization. ACS Applied Electronic Materials, 2020, 2, 1090-1098.	2.0	59
156	Preparation of YAG:Nd nano-sized powder by co-precipitation method. Materials Science & Engineering A: Structural Materials: Properties, Microstructure and Processing, 2004, 379, 347-350.	2.6	58
157	Genome Sequence of the Halotolerant Marine Bacterium Myxococcus fulvus HW-1. Journal of Bacteriology, 2011, 193, 5015-5016.	1.0	57
158	TiO <sub>2</sub> Nanorod Array Constructed Nanotopography for Regulation of Mesenchymal Stem Cells Fate and the Realization of Location ommitted Stem Cell Differentiation. Small, 2016, 12, 1770-1778.	5.2	57
159	Growth and investigation of a new nonlinear optical crystal: bismuth borate BiB3O6. Journal of Crystal Growth, 2001, 224, 280-283.	0.7	56
160	Synthesis of Nd3+ doped nano-crystalline yttrium aluminum garnet (YAG) powders leading to transparent ceramic. Optical Materials, 2007, 29, 528-531.	1.7	56
161	Nanopaper based on Ag/TiO2 nanobelts heterostructure for continuous-flow photocatalytic treatment of liquid and gas phase pollutants. Journal of Hazardous Materials, 2011, 197, 19-25.	6.5	56
162	Carbodiimide crosslinked collagen from porcine dermal matrix for high-strength tissue engineering scaffold. International Journal of Biological Macromolecules, 2013, 61, 69-74.	3.6	56

#	Article	IF	CITATIONS
163	MoSe <sub>2</sub> nanosheet/MoO <sub>2</sub> nanobelt/carbon nanotube membrane as flexible and multifunctional electrodes for full water splitting in acidic electrolyte. Nanoscale, 2018, 10, 9268-9275.	2.8	56
164	Construction of bimetallic Pd-Ag enhanced AgBr/TiO2 hierarchical nanostructured photocatalytic hybrid capillary tubes and devices for continuous photocatalytic degradation of VOCs. Chemical Engineering Journal, 2018, 346, 77-84.	6.6	56
165	Electromagnetic induction derived micro-electric potential in metal-semiconductor core-shell hybrid nanostructure enhancing charge separation for high performance photocatalysis. Nano Energy, 2020, 71, 104624.	8.2	56
166	Tailoring Local Electrolyte Solvation Structure via a Mesoporous Molecular Sieve for Dendriteâ€Free Zinc Batteries. Advanced Functional Materials, 2022, 32, .	7.8	56
167	Growth of Yb:YAl3(BO3)4 crystals and their optical and self-frequency-doubling properties. Journal of Crystal Growth, 2001, 233, 248-252.	0.7	55
168	Interface dominated high photocatalytic properties of electrostatic self-assembled Ag2O/TiO2 heterostructure. Physical Chemistry Chemical Physics, 2010, 12, 15119.	1.3	55
169	One-pot synthesis of nitrogen-doped TiO2 nanorods with anatase/brookite structures and enhanced photocatalytic activity. CrystEngComm, 2012, 14, 7662.	1.3	55
170	Bioactivity of periodontal ligament stem cells on sodium titanate coated with graphene oxide. Scientific Reports, 2016, 6, 19343.	1.6	55
171	RuO2/TiO2 nanobelt heterostructures with enhanced photocatalytic activity and gas-phase selective oxidation of benzyl alcohol. Solar Energy Materials and Solar Cells, 2016, 151, 7-13.	3.0	55
172	Weaker Interactions in Zn <sup>2+</sup> and Organic Ionâ€preâ€intercalated Vanadium Oxide toward Highly Reversible Zincâ€ion Batteries. Energy and Environmental Materials, 2021, 4, 620-630.	7.3	55
173	Production of Nanosized YAG Powders with Spherical Morphology and Nonaggregation via a Solvothermal Method. Journal of the American Ceramic Society, 2004, 87, 2288-2290.	1.9	54
174	A high performance quasi-solid-state self-powered UV photodetector based on TiO <sub>2</sub> nanorod arrays. Nanoscale, 2014, 6, 9116.	2.8	54
175	One-step synthesis of ultrathin nanobelts-assembled urchin-like anatase TiO <sub>2</sub> nanostructures for highly efficient photocatalysis. CrystEngComm, 2017, 19, 129-136.	1.3	54
176	High-quality 2-μm Q-switched pulsed solid-state lasers using spin-coating-coreduction approach synthesized Bi <sub>2</sub> Te <sub>3</sub> topological insulators. Photonics Research, 2018, 6, 314.	3.4	54
177	Highly-efficient overall water splitting in 2D Janus group-III chalcogenide multilayers: the roles of intrinsic electric filed and vacancy defects. Science Bulletin, 2020, 65, 27-34.	4.3	54
178	A Microorganism Bred TiO <sub>2</sub> /Au/TiO <sub>2</sub> Heterostructure for Whispering Gallery Mode Resonance Assisted Plasmonic Photocatalysis. ACS Nano, 2020, 14, 13876-13885.	7.3	54
179	Chemical assembly of silver nanoparticles on stainless steel for antimicrobial applications. Surface and Coatings Technology, 2010, 204, 3871-3875.	2.2	53
180	High-performance TiO2 from Baker's yeast. Journal of Colloid and Interface Science, 2011, 354, 109-115.	5.0	53

#	Article	IF	CITATIONS
181	In situ construction of a titanate–silver nanoparticle–titanate sandwich nanostructure on a metallic titanium surface for bacteriostatic and biocompatible implants. Journal of Materials Chemistry, 2012, 22, 19151.	6.7	53
182	UV-visible-light-activated photocatalysts based on Bi2O3/Bi4Ti3O12/TiO2 double-heterostructured TiO2 nanobelts. Journal of Materials Chemistry, 2012, 22, 23395.	6.7	53
183	Growth and accelerated differentiation of mesenchymal stem cells on graphene-oxide-coated titanate with dexamethasone on surface of titanium implants. Dental Materials, 2017, 33, 525-535.	1.6	53
184	Editable TiO <sub>2</sub> Nanomaterial-Modified Paper in Situ for Highly Efficient Detection of Carcinoembryonic Antigen by Photoelectrochemical Method. ACS Applied Materials & Interfaces, 2018, 10, 14594-14601.	4.0	52
185	Tungsten boride: a 2D multiple Dirac semimetal for the hydrogen evolution reaction. Journal of Materials Chemistry C, 2019, 7, 8868-8873.	2.7	52
186	Wireless Localized Electrical Stimulation Generated by an Ultrasoundâ€Driven Piezoelectric Discharge Regulates Proinflammatory Macrophage Polarization. Advanced Science, 2021, 8, 2100962.	5.6	52
187	Superâ€Hybrid Transition Metal Sulfide Nanoarrays of Co <sub>3</sub> S <sub>4</sub> Nanosheet/Pâ€Doped WS <sub>2</sub> Nanosheet/Co <sub>9</sub> S <sub>8</sub> Nanoparticle with Ptâ€Like Activities for Robust Allâ€pH Hydrogen Evolution. Advanced Functional Materials, 2022, 32, .	7.8	52
188	Building Ag nanoparticle 3D catalyst via Na2Ti3O7 nanowires for the detection of hydrogen peroxide. Sensors and Actuators B: Chemical, 2010, 144, 289-294.	4.0	51
189	One-Dimensional Hydroxyapatite Nanostructures with Tunable Length for Efficient Stem Cell Differentiation Regulation. ACS Applied Materials & Interfaces, 2017, 9, 33717-33727.	4.0	51
190	General Approach to the Synthesis of Heterodimers of Metal Nanoparticles through Site-Selected Protection and Growth. Nano Letters, 2019, 19, 6703-6708.	4.5	51
191	Assembling Sn3O4 nanostructures on a hydrophobic PVDF film through metal-F coordination to construct a piezotronic effect-enhanced Sn3O4/PVDF hybrid photocatalyst. Nano Energy, 2020, 72, 104688.	8.2	51
192	Electron Spin Polarization-Enhanced Photoinduced Charge Separation in Ferromagnetic ZnFe <sub>2</sub> O <sub>4</sub> . ACS Energy Letters, 2021, 6, 2129-2137.	8.8	51
193	Constructing van der Waals Heterogeneous Photocatalysts Based on Atomically Thin Carbon Nitride Sheets and Graphdiyne for Highly Efficient Photocatalytic Conversion of CO <sub>2</sub> into CO. ACS Applied Materials & Interfaces, 2021, 13, 40629-40637.	4.0	51
194	Killing two birds with one stone: To eliminate the toxicity and enhance the photocatalytic property of CdS nanobelts by assembling ultrafine TiO2 nanowires on them. Solar Energy Materials and Solar Cells, 2018, 183, 41-47.	3.0	50
195	Mechanoluminescence enhancement of ZnS:Cu,Mn with piezotronic effect induced trap-depth reduction originated from PVDF ferroelectric film. Nano Energy, 2019, 63, 103861.	8.2	50
196	Multi-interfacial engineering of hierarchical CoNi2S4/WS2/Co9S8 hybrid frameworks for robust all-pH electrocatalytic hydrogen evolution. Applied Catalysis B: Environmental, 2021, 297, 120455.	10.8	50
197	Crystal growth, thermal and optical performance of BiB3O6. Journal of Crystal Growth, 2001, 233, 282-286.	0.7	49
198	Sonochemical synthesis of bismuth selenide nanobelts at room temperature. Journal of Crystal Growth, 2004, 271, 456-461.	0.7	49

#	Article	IF	CITATIONS
199	Synthesis and characterization of SnSe2 hexagonal nanoflakes. Materials Letters, 2009, 63, 512-514.	1.3	49
200	Nanostructured Titanate with Different Metal Ions on the Surface of Metallic Titanium: A Facile Approach for Regulation of rBMSCs Fate on Titanium Implants. Small, 2014, 10, 3169-3180.	5.2	49
201	Nanotechnology for Neuroscience: Promising Approaches for Diagnostics, Therapeutics and Brain Activity Mapping. Advanced Functional Materials, 2017, 27, 1700489.	7.8	49
202	Synthesis and thermoelectric properties of Bi2O2Se nanosheets. Materials Research Bulletin, 2013, 48, 3968-3972.	2.7	48
203	A Facile and Effective Method for Patching Sulfur Vacancies of WS <sub>2</sub> via Nitrogen Plasma Treatment. Small, 2019, 15, e1901791.	5.2	48
204	An earth-abundant and multifunctional Ni nanosheets array as electrocatalysts and heat absorption layer integrated thermoelectric device for overall water splitting. Nano Energy, 2019, 56, 563-570.	8.2	48
205	Poly- <scp>l</scp> -Lysine-Modified Graphene Field-Effect Transistor Biosensors for Ultrasensitive Breast Cancer miRNAs and SARS-CoV-2 RNA Detection. Analytical Chemistry, 2022, 94, 1626-1636.	3.2	48
206	Rapid synthesis of YAG nano-sized powders by a novel method. Materials Letters, 2004, 58, 2377-2380.	1.3	47
207	Synthesis, structure, and piezoelectric properties of ferroelectric and antiferroelectric NaNbO <sub>3</sub> nanostructures. CrystEngComm, 2014, 16, 7598-7604.	1.3	47
208	UV-Irradiation-Enhanced Ferromagnetism in BaTiO <sub>3</sub> . Journal of Physical Chemistry Letters, 2010, 1, 238-241.	2.1	46
209	Construction of A Fluorescent Nanostructured Chitosan-Hydroxyapatite Scaffold by Nanocrystallon Induced Biomimetic Mineralization and Its Cell Biocompatibility. ACS Applied Materials & Interfaces, 2011, 3, 1692-1701.	4.0	46
210	Enhanced decoloration activity by Cu2O@TiO2 nanobelts heterostructures via a strong adsorption-weak photodegradation process. Applied Surface Science, 2013, 282, 84-91.	3.1	46
211	TiO2 particles wrapped onto macroporous germanium skeleton as high performance anode for lithium-ion batteries. Chemical Engineering Journal, 2020, 381, 122649.	6.6	46
212	Synthesis of Wafer cale Graphene with Chemical Vapor Deposition for Electronic Device Applications. Advanced Materials Technologies, 2021, 6, 2000744.	3.0	46
213	A Nanostructured Molybdenum Disulfide Film for Promoting Neural Stem Cell Neuronal Differentiation: toward a Nerve Tissueâ€Engineered 3D Scaffold. Advanced Biology, 2017, 1, e1600042.	3.0	45
214	Ultrafine Si nanowires/Sn3O4 nanosheets 3D hierarchical heterostructured array as a photoanode with high-efficient photoelectrocatalytic performance. Applied Catalysis B: Environmental, 2019, 256, 117798.	10.8	45
215	Graphene Biodevices for Early Disease Diagnosis Based on Biomarker Detection. ACS Sensors, 2021, 6, 3841-3881.	4.0	45
216	Applications of nanogenerators for biomedical engineering and healthcare systems. InformaÄnÃ- Materiály, 2022, 4, .	8.5	45

#	Article	IF	CITATIONS
217	Nitrogen-doped In2O3 nanocrystals constituting hierarchical structures with enhanced gas-sensing properties. CrystEngComm, 2012, 14, 7479.	1.3	44
218	Exopolysaccharide microchannels direct bacterial motility and organize multicellular behavior. ISME Journal, 2016, 10, 2620-2632.	4.4	44
219	Using cellulose fibers to fabricate transparent paper by microfibrillation. Carbohydrate Polymers, 2019, 214, 26-33.	5.1	44
220	Attomolar-Level Ultrasensitive and Multiplex microRNA Detection Enabled by a Nanomaterial Locally Assembled Microfluidic Biochip for Cancer Diagnosis. Analytical Chemistry, 2021, 93, 5129-5136.	3.2	44
221	Growth of Bi2Se3Nanobelts Synthesized through a Co-Reduction Method under Ultrasonic Irradiation at Room Temperature. Crystal Growth and Design, 2005, 5, 1711-1714.	1.4	43
222	Controlled Synthesis of Hydrogen Titanateâ^'Polyaniline Composite Nanowires and Their Resistanceâ^'Temperature Characteristics. Journal of Physical Chemistry C, 2009, 113, 7610-7615.	1.5	43
223	Photoresponsive nanostructure assisted green synthesis of organics and polymers. Applied Catalysis B: Environmental, 2019, 249, 172-210.	10.8	43
224	One-pot synthesis of BiOCl nanosheets with dual functional carbon for ultra-highly efficient photocatalytic degradation of RhB. Environmental Research, 2020, 182, 109077.	3.7	43
225	In Situ Electrochemical Transformation Reaction of Ammonium-Anchored Heptavanadate Cathode for Long-Life Aqueous Zinc-Ion Batteries. ACS Applied Materials & Interfaces, 2021, 13, 5034-5043.	4.0	43
226	Underfocus Laser Induced Ni Nanoparticles Embedded Metallic MoN Microrods as Patterned Electrode for Efficient Overall Water Splitting. Advanced Science, 2022, 9, e2105869.	5.6	43
227	Mechanistic Insight into the Function of the C-terminal PKD Domain of the Collagenolytic Serine Protease Deseasin MCP-01 from Deep Sea Pseudoalteromonas sp. SM9913. Journal of Biological Chemistry, 2010, 285, 14285-14291.	1.6	42
228	Synthesis and visible-light photocatalytic activity of NdVO4 nanowires. Journal of Alloys and Compounds, 2011, 509, 7968-7972.	2.8	42
229	Solvothermal synthesis and luminescent properties of YAG:Tb nano-sized phosphors. Journal of Physics and Chemistry of Solids, 2005, 66, 201-205.	1.9	41
230	A rapid-response humidity sensor based on BaNbO3 nanocrystals. Sensors and Actuators B: Chemical, 2009, 136, 128-132.	4.0	41
231	Eu/Tb codoped spindle-shaped fluorinated hydroxyapatite nanoparticles for dual-color cell imaging. Nanoscale, 2016, 8, 11580-11587.	2.8	41
232	Active facet regulation of highly aligned molybdenum carbide porous octahedrons via crystal engineering for hydrogen evolution reaction. Nano Energy, 2020, 77, 105056.	8.2	41
233	Fabrication of a Sensitive Strain and Pressure Sensor from Gold Nanoparticle-Assembled 3D-Interconnected Graphene Microchannel-Embedded PDMS. ACS Applied Materials & Interfaces, 2020, 12, 51854-51863.	4.0	41
234	Strategies of structural and defect engineering for high-performance rechargeable aqueous zinc-ion batteries. Journal of Materials Chemistry A, 2021, 9, 19245-19281.	5.2	41

#	Article	IF	CITATIONS
235	High ethanol sensitivity of Palladium/TiO2 nanobelt surface heterostructures dominated by enlarged surface area and nano-Schottky junctions. Journal of Colloid and Interface Science, 2012, 388, 144-150.	5.0	40
236	Solar driven electrochromic photoelectrochemical fuel cells for simultaneous energy conversion, storage and self-powered sensing. Nanoscale, 2018, 10, 3421-3428.	2.8	40
237	Excitation Management of Lead-Free Perovskite Nanocrystals Through Doping. ACS Applied Materials & Interfaces, 2021, 13, 6404-6410.	4.0	40
238	Graphene oxide-graphene Van der Waals heterostructure transistor biosensor for SARS-CoV-2 protein detection. Talanta, 2022, 240, 123197.	2.9	40
239	Strong Interaction over Ru/Defectsâ€Rich Aluminium Oxide Boosts Photothermal CO <sub>2</sub> Methanation via Microchannel Flowâ€Type System. Advanced Energy Materials, 2022, 12, .	10.2	40
240	Novel synthesis of YAG by solvothermal method. Journal of Crystal Growth, 2005, 275, e1913-e1917.	0.7	39
241	Construction of titanium dioxide nanorod/graphite microfiber hybrid electrodes for a high performance electrochemical glucose biosensor. Nanoscale, 2016, 8, 9382-9389.	2.8	39
242	Structure and electronic transport properties of polyaniline/NaFe4P12 composite. Chemical Physics Letters, 2002, 352, 185-190.	1.2	38
243	A stable bimetallic Au–Ag/TiO2 nanopaper for aerobic oxidation of benzyl alcohol. Chemical Communications, 2013, 49, 11524.	2.2	38
244	TiO2 nanorod arrays modified Ti substrates promote the adhesion, proliferation and osteogenic differentiation of human periodontal ligament stem cells. Materials Science and Engineering C, 2017, 76, 684-691.	3.8	38
245	MoC nanoclusters anchored Ni@Nâ€doped carbon nanotubes coated on carbon fiber as threeâ€dimensional and multifunctional electrodes for flexible supercapacitor and selfâ€heating device. , 2021, 3, 129-141.		38
246	Advancing Versatile Ferroelectric Materials Toward Biomedical Applications. Advanced Science, 2021, 8, 2003074.	5.6	38
247	Synthesis of CdS/MoS <sub>2</sub> Nanooctahedrons Heterostructure with a Tight Interface for Enhanced Photocatalytic H <sub>2</sub> Evolution and Biomass Upgrading. Solar Rrl, 2021, 5, 2000415.	3.1	38
248	Synergistic catalysis of Au–Cu/TiO <sub>2</sub> -NB nanopaper in aerobic oxidation of benzyl alcohol. Journal of Materials Chemistry A, 2014, 2, 16292-16298.	5.2	37
249	Highly Efficient Photocatalysts and Continuousâ€Flow Photocatalytic Reactors for Degradation of Organic Pollutants in Wastewater. Chemistry - an Asian Journal, 2016, 11, 2352-2371.	1.7	37
250	Optical nonlinearity engineering of a bismuth telluride saturable absorber and application of a pulsed solid state laser therein. Nanoscale, 2017, 9, 19100-19107.	2.8	37
251	Prolonged fluorescence lifetime of carbon quantum dots by combining with hydroxyapatite nanorods for bio-applications. Nanoscale, 2017, 9, 2162-2171.	2.8	37
252	Nanostructured molybdenum disulfide biointerface for adhesion and osteogenic differentiation of mesenchymal stem cells. Applied Materials Today, 2018, 10, 164-172.	2.3	37

#	Article	IF	CITATIONS
253	Top or Bottom, Assembling Modules Determine the Photocatalytic Property of the Sheetlike Nanostructured Hybrid Photocatalyst Composed with Sn <sub>3</sub> O <sub>4</sub> and rGO (GQD). ACS Sustainable Chemistry and Engineering, 2018, 6, 11775-11782.	3.2	37
254	N-Doped Mo2C Nanobelts/Graphene Nanosheets Bonded with Hydroxy Nanocellulose as Flexible and Editable Electrode for Hydrogen Evolution Reaction. IScience, 2019, 19, 1090-1100.	1.9	37
255	Raman spectroscopy investigation of partially filled skutterudite. Chemical Physics Letters, 2001, 347, 373-377.	1.2	36
256	Growth, optical and thermal properties of near-stoichiometric LiNbO3 single crystal. Journal of Alloys and Compounds, 2008, 455, 501-505.	2.8	36
257	Synthesis and characterization of Cu2Se prepared by hydrothermal co-reduction. Journal of Alloys and Compounds, 2009, 484, 674-676.	2.8	36
258	In vitro Investigation on the Biodegradability and Biocompatibility of Genipin Cross-linked Porcine Acellular Dermal Matrix with Intrinsic Fluorescence. ACS Applied Materials & Interfaces, 2013, 5, 344-350.	4.0	36
259	Partial wet route for YAG powders synthesis leading to transparent ceramic: A core–shell solid-state reaction process. Journal of the European Ceramic Society, 2013, 33, 2617-2623.	2.8	36
260	Progress in miRNA Detection Using Graphene Material–Based Biosensors. Small, 2019, 15, e1901867.	5.2	36
261	A Series of Carbazole Cationic Compounds with Large Two-Photon Absorption Cross Sections for Imaging Mitochondria in Living Cells with Two-Photon Fluorescence Microscopy. Journal of Fluorescence, 2011, 21, 497-506.	1.3	35
262	Ammonium sulfate regulation of morphology of Nd:Y2O3 precursor via urea precipitation method and its effect on the sintering properties of Nd:Y2O3 nanopowders. CrystEngComm, 2012, 14, 1783.	1.3	35
263	Synthesis of nano-sized and highly sinterable Nd:YAG powders by the urea homogeneous precipitation method. Powder Technology, 2012, 217, 140-147.	2.1	35
264	Piezoelectric nylon-11 nanoparticles with ultrasound assistance for high-efficiency promotion of stem cell osteogenic differentiation. Journal of Materials Chemistry B, 2019, 7, 1847-1854.	2.9	35
265	Piezopotential gated two-dimensional InSe field-effect transistor for designing a pressure sensor based on piezotronic effect. Nano Energy, 2020, 70, 104457.	8.2	35
266	Puffing quaternary FexCoyNi1-x-yP nanoarray via kinetically controlled alkaline etching for robust overall water splitting. Science China Materials, 2020, 63, 1054-1064.	3.5	35
267	Regulation of stem cell fate using nanostructure-mediated physical signals. Chemical Society Reviews, 2021, 50, 12828-12872.	18.7	35
268	Biocarbon-coated LiFePO4 nucleus nanoparticles enhancing electrochemical performances. Chemical Communications, 2012, 48, 10093.	2.2	34
269	Phosphorusâ€Doped Iron Nitride Nanoparticles Encapsulated by Nitrogenâ€Doped Carbon Nanosheets on Iron Foam In Situ Derived from <i>Saccharomycetes Cerevisiae</i> for Electrocatalytic Overall Water Splitting. Small, 2020, 16, e2001980.	5.2	34
270	Continuous-wave tri-wavelength operation at 1064, 1319 and 1338 nm of LD end-pumped Nd:YAG ceramic laser. Optics Express, 2010, 18, 22167.	1.7	33

#	Article	IF	CITATIONS
271	<i>In vitro</i> Biomimetic Construction of Hydroxyapatite–Porcine Acellular Dermal Matrix Composite Scaffold for MC3T3-E1 Preosteoblast Culture. Tissue Engineering - Part A, 2011, 17, 765-776.	1.6	33
272	Bismuth titanate nanobelts through a low-temperature nanoscale solid-state reaction. Acta Materialia, 2014, 62, 258-266.	3.8	33
273	Hot Hole Enhanced Synergistic Catalytic Oxidation on Pt u Alloy Clusters. Advanced Science, 2017, 4, 1600448.	5.6	33
274	In situ alternative switching between Ti <sup>4+</sup> and Ti <sup>3+</sup> driven by H <sub>2</sub> O <sub>2</sub> in TiO <sub>2</sub> nanostructures: mechanism of pseudo-Fenton reaction. Materials Chemistry Frontiers, 2017, 1, 1989-1994.	3.2	33
275	Graphene quantum dots modified nanoporous SiAl composite as an advanced anode for lithium storage. Electrochimica Acta, 2019, 318, 228-235.	2.6	33
276	Electrochemically Exfoliated Chlorineâ€Doped Graphene for Flexible Allâ€Solidâ€State Microâ€Supercapacitors with High Volumetric Energy Density. Advanced Materials, 2022, 34, e2106309.	11.1	33
277	Carrier Step-by-Step Transport Initiated by Precise Defect Distribution Engineering for Efficient Photocatalytic Hydrogen Generation. ACS Applied Materials & Interfaces, 2017, 9, 4634-4642.	4.0	32
278	PdO/TiO2 nanobelt heterostructures with high photocatalytic activities based on an exposed highly active facet on ultrathin TiO2 nanobelts. Solar Energy Materials and Solar Cells, 2017, 161, 297-304.	3.0	32
279	Construction of High Field-Effect Mobility Multilayer MoS2 Field-Effect Transistors with Excellent Stability through Interface Engineering. ACS Applied Electronic Materials, 2020, 2, 2132-2140.	2.0	32
280	Highâ€performance electronics and optoelectronics of monolayer tungsten diselenide full film from preâ€seeding strategy. InformaÄnÃ-Materiály, 2021, 3, 1455-1469.	8.5	32
281	Gram-scale wet chemical synthesis of Ag2O/TiO2 aggregated sphere heterostructure with high photocatalytic activity. Materials Letters, 2013, 91, 81-83.	1.3	31
282	Effects of Eu3+ and Dy3+ doping or co-doping on optical and structural properties of BaB2Si2O8 phosphor for white LED applications. Journal of Rare Earths, 2016, 34, 21-29.	2.5	31
283	Stable InSe transistors with high-field effect mobility for reliable nerve signal sensing. Npj 2D Materials and Applications, 2019, 3, .	3.9	31
284	The study of surfactant application on synthesis of YAG nano-sized powders. Powder Technology, 2006, 163, 202-205.	2.1	30
285	Electrodeposition of submicron/nanoscale Cu2O/Cu junctions in an ultrathin CuSO4 solution layer. Journal of Electroanalytical Chemistry, 2010, 638, 225-230.	1.9	30
286	<i>Myxococcus xanthus</i> Viability Depends on GroEL Supplied by Either of Two Genes, but the Paralogs Have Different Functions during Heat Shock, Predation, and Development. Journal of Bacteriology, 2010, 192, 1875-1881.	1.0	30
287	Chemical composition evolution of YAG co-precipitate determined by pH during aging period and its effect on precursor properties. Ceramics International, 2012, 38, 1635-1641.	2.3	30
288	The dielectric and photochromic properties of defect-rich BaTiO3 microcrystallites synthesized from Ti2O3. Materials Science and Engineering B: Solid-State Materials for Advanced Technology, 2012, 177, 639-644.	1.7	30

#	Article	IF	CITATIONS
289	Synthesis and magnetic properties of Sn1â^'Co O2 nanostructures and their application in gas sensing. Sensors and Actuators B: Chemical, 2013, 184, 288-294.	4.0	30
290	TiO <sub>2</sub> /TiN core/shell nanobelts for efficient solar hydrogen generation. Chemical Communications, 2018, 54, 6056-6059.	2.2	30
291	Microflowers Comprised of Cu/Cu <sub><i>x</i></sub> O/NC Nanosheets as Electrocatalysts and Horseradish Peroxidase Mimics. ACS Applied Nano Materials, 2020, 3, 617-623.	2.4	30
292	Enrichment-Detection Integrated Exosome Profiling Biosensors Promising for Early Diagnosis of Cancer. Analytical Chemistry, 2021, 93, 4697-4706.	3.2	30
293	Influence of annealing on ZnO films grown by metal–organic chemical vapor deposition. Materials Letters, 2004, 58, 3630-3633.	1.3	29
294	An experimental study: Thermal performance of molten salt cavity receivers. Applied Thermal Engineering, 2013, 50, 334-341.	3.0	29
295	Sustained delivery of BMP-2 enhanced osteoblastic differentiation of BMSCs based on surface hydroxyapatite nanostructure in chitosan–HAp scaffold. Journal of Biomaterials Science, Polymer Edition, 2014, 25, 1813-1827.	1.9	29
296	Hierarchical nested-network porous copper fabricated by one-step dealloying for glucose sensing. Journal of Alloys and Compounds, 2016, 681, 109-114.	2.8	29
297	Ru nanoparticles decorated TiO 2 nanobelts: A heterostructure towards enhanced photocatalytic activity and gas-phase selective oxidation of benzyl alcohol. Ceramics International, 2016, 42, 1611-1617.	2.3	29
298	Non-thermal radiation heating synthesis of nanomaterials. Science Bulletin, 2021, 66, 386-406.	4.3	29
299	Ultrasonic-driven electrical signal-iron ion synergistic stimulation based on piezotronics induced neural differentiation of mesenchymal stem cells on FeOOH/PVDF nanofibrous hybrid membrane. Nano Energy, 2021, 87, 106192.	8.2	29
300	Nanostructured Black Aluminum Prepared by Laser Direct Writing as a High-Performance Plasmonic Absorber for Photothermal/Electric Conversion. ACS Applied Materials & Interfaces, 2021, 13, 4305-4315.	4.0	29
301	Optical transition properties of Er3+ions in YAl3(BO3)4 crystal. Chemical Physics Letters, 2002, 365, 279-284.	1.2	28
302	Room-temperature synthesis and high visible-light-induced photocatalytic activity of AgI/BiOI composites. Journal of Environmental Chemical Engineering, 2013, 1, 526-533.	3.3	28
303	Edge dominated electronic properties of MoS <sub>2</sub> /graphene hybrid 2D materials: edge state, electron coupling and work function. Journal of Materials Chemistry C, 2017, 5, 4845-4851.	2.7	28
304	Mass-production of fluorescent chitosan/graphene oxide hybrid microspheres for in vitro 3D expansion of human umbilical cord mesenchymal stem cells. Chemical Engineering Journal, 2018, 331, 675-684.	6.6	28
305	An Ultrafast Selfâ€Polarization Effect in Barium Titanate Filled Poly(Vinylidene Fluoride) Composite Film Enabled by Selfâ€Charge Excitation Triboelectric Nanogenerator. Advanced Functional Materials, 2022, 32, .	7.8	28
306	Passively Q-switched dual-wavelength laser output of LD-end-pumped ceramic Nd:YAG laser. Optics Express, 2009, 17, 12076.	1.7	27

#	Article	IF	CITATIONS
307	ZnS nanoparticles self-assembled from ultrafine particles and their highly photocatalytic activity. Physica E: Low-Dimensional Systems and Nanostructures, 2011, 43, 1071-1075.	1.3	27
308	Three-dimensional CdS nanostructure for photoelectrochemical sensor. Sensors and Actuators B: Chemical, 2013, 182, 461-466.	4.0	27
309	Mechanisms Involved in the Functional Divergence of Duplicated GroEL Chaperonins in Myxococcus xanthus DK1622. PLoS Genetics, 2013, 9, e1003306.	1.5	27
310	Broadband light-concentration with near-surface distribution by silver capped silicon nanowire for high-performance solar cells. Nano Energy, 2015, 11, 756-764.	8.2	27
311	Terbium–Aspartic Acid Nanocrystals with Chirality-Dependent Tunable Fluorescent Properties. ACS Nano, 2017, 11, 1973-1981.	7.3	27
312	Cellular Stemness Maintenance of Human Adiposeâ€Đerived Stem Cells on ZnO Nanorod Arrays. Small, 2019, 15, e1904099.	5.2	27
313	Commercially Available CuO Catalyzed Hydrogenation of Nitroarenes Using Ammonia Borane as a Hydrogen Source. ChemCatChem, 2020, 12, 2426-2430.	1.8	27
314	Optical and thermal properties of nonlinear optical crystal LaCa4O(BO3)3. Chemical Physics Letters, 2003, 372, 788-793.	1.2	26
315	Co-cultivation of <i>Sorangium cellulosum</i> strains affects cellular growth and biosynthesis of secondary metabolite epothilones. FEMS Microbiology Ecology, 2013, 85, 358-368.	1.3	26
316	In situ fabrication of silver nanoparticle-filled hydrogen titanate nanotube layer on metallic titanium surface for bacteriostatic and biocompatible implantation. International Journal of Nanomedicine, 2013, 8, 2903.	3.3	26
317	Bright YAG:Ce Nanorod Phosphors Prepared via a Partial Wet Chemical Route and Biolabeling Applications. ACS Applied Materials & Interfaces, 2016, 8, 11990-11997.	4.0	26
318	A novel aptameric biosensor based on the self-assembled DNA–WS2 nanosheet architecture. Talanta, 2017, 163, 78-84.	2.9	26
319	Hydroxyapatite nanowires modified polylactic acid membrane plays barrier/osteoinduction dual roles and promotes bone regeneration in a rat mandible defect model. Journal of Biomedical Materials Research - Part A, 2018, 106, 3099-3110.	2.1	26
320	Boosting Electrochemistry of Manganese Oxide Nanosheets by Ostwald Ripening during Reduction for Fiber Electrochemical Energy Storage Device. ACS Applied Materials & Interfaces, 2018, 10, 30388-30399.	4.0	26
321	Two-photon absorption within layered Bi <sub>2</sub> Te <sub>3</sub> topological insulators and the role of nonlinear transmittance therein. Journal of Materials Chemistry C, 2019, 7, 7027-7034.	2.7	26
322	Efficiently degradation of polyacrylamide pollution using a full spectrum Sn3O4 nanosheet/Ni foam heterostructure photoelectrocatalyst. Catalysis Today, 2019, 335, 520-526.	2.2	26
323	One-Step Sublimation and Epitaxial Growth of CdS-Cd Heterogeneous Nanoparticles on S-Doped MoO <sub>2</sub> Nanosheets for Efficient Visible Light-Driven Photocatalytic H <sub>2</sub> Generation. ACS Applied Materials & Interfaces, 2020, 12, 2362-2369.	4.0	26
324	Addressable surface engineering for N-doped WS <sub>2</sub> nanosheet arrays with abundant active sites and the optimal local electronic structure for enhanced hydrogen evolution reaction. Nanoscale, 2020, 12, 22541-22550.	2.8	26

#	Article	IF	CITATIONS
325	Revisiting the nanocrystal formation process of zero-dimensional perovskite. Journal of Materials Chemistry A, 2021, 9, 4658-4663.	5.2	26
326	Ultrasensitive and stable all graphene fieldâ€effect transistorâ€based Hg <sup>2+</sup> sensor constructed by using different covalently bonded RGO films assembled by different conjugate linking molecules. SmartMat, 2021, 2, 213-225.	6.4	26
327	Yttrium aluminum garnet nanoparticles synthesized by nitrate decomposition and their low temperature densification behavior. Journal of Alloys and Compounds, 2010, 490, 459-462.	2.8	25
328	Raspite PbWO4 nanobelts: synthesis and properties. CrystEngComm, 2010, 12, 3277.	1.3	25
329	Highly conductive and bendable gold networks attached on intertwined cellulose fibers for output controllable power paper. Journal of Materials Chemistry A, 2018, 6, 19611-19620.	5.2	25
330	Support-free 3D hierarchical nanoporous Cu@Cu2O for fast tandem ammonia borane dehydrogenation and nitroarenes hydrogenation under mild conditions. Journal of Alloys and Compounds, 2020, 815, 152372.	2.8	25
331	Biomimetic Metalâ^'Organic Frameworks as Targeted Vehicles to Enhance Osteogenesis. Advanced Healthcare Materials, 2022, 11, e2102821.	3.9	25
332	Improving conjugation efficacy of Sorangium cellulosum by the addition of dual selection antibiotics. Journal of Industrial Microbiology and Biotechnology, 2008, 35, 1157-1163.	1.4	24
333	A full-spectrum photocatalyst with strong near-infrared photoactivity derived from synergy of nano-heterostructured Er <sup>3+</sup> -doped multi-phase oxides. Nanoscale, 2017, 9, 18940-18950.	2.8	24
334	Tuning Longâ€Lived Mn(II) Upconversion Luminescence through Alkalineâ€Earth Metal Doping and Energyâ€Level Tailoring. Advanced Optical Materials, 2019, 7, 1900519.	3.6	24
335	Plasmon enhanced upconverting core@triple-shell nanoparticles as recyclable panchromatic initiators (blue to infrared) for radical polymerization. Nanoscale Horizons, 2019, 4, 907-917.	4.1	24
336	Integrating NiMoO wafer as a heterogeneous â€~turbo' for engineering robust Ru-based electrocatalyst for overall water splitting. Chemical Engineering Journal, 2021, 420, 127686.	6.6	24
337	Anisotropic thermal expansion of BiB3O6. Journal of Applied Physics, 2002, 91, 3618-3620.	1.1	23
338	Bismuth Spheres Grown in Self-Nested Cavities in a Silicon Wafer. Journal of the American Chemical Society, 2005, 127, 15322-15326.	6.6	23
339	Effects of aging on the characteristics of Nd:YAG nano-powders. Journal of Alloys and Compounds, 2010, 502, 206-210.	2.8	23
340	Micropatterning of the Ferroelectric Phase in a Poly(vinylidene difluoride) Film by Plasmonic Heating with Gold Nanocages. Angewandte Chemie - International Edition, 2016, 55, 13828-13832.	7.2	23
341	Surgical Sutures with Porous Sheaths for the Sustained Release of Growth Factors. Advanced Materials, 2016, 28, 4620-4624.	11.1	23
342	Unsymmetrical Alveolate PMMA/MWCNT Film as a Piezoresistive E-Skin with Four-Dimensional Resolution and Application for Detecting Motion Direction and Airflow Rate. ACS Applied Materials & Interfaces, 2020, 12, 30896-30904.	4.0	23

#	Article	IF	CITATIONS
343	A Universal Process: Self-Templated and Orientated Fabrication of XMoO <sub>4</sub> (X: Ni, Co, or Fe) Nanosheets on MoO <sub>2</sub> Nanoplates as Electrocatalysts for Efficient Water Splitting. ACS Applied Materials & Interfaces, 2020, 12, 33785-33794.	4.0	23
344	Emerging Internet of Things driven carbon nanotubes-based devices. Nano Research, 2022, 15, 4613-4637.	5.8	23
345	BaTiO3 nanocubes: Size-selective formation and structure analysis. Materials Letters, 2008, 62, 235-238.	1.3	22
346	<i>Hdsp</i> , a horizontally transferred gene required for social behavior and halotolerance in salt-tolerant <i>Myxococcus fulvus</i> HW-1. ISME Journal, 2010, 4, 1282-1289.	4.4	22
347	High-performance wearable supercapacitors fabricated with surface activated continuous filament graphite fibers. Journal of Power Sources, 2017, 358, 13-21.	4.0	22
348	A titanium dioxide nanorod array as a high-affinity nano-bio interface of a microfluidic device for efficient capture of circulating tumor cells. Nano Research, 2017, 10, 776-784.	5.8	22
349	Low Lattice Mismatch InSe–Se Vertical Van der Waals Heterostructure for Highâ€performance Transistors via Strong Fermiâ€Level Depinning. Small Methods, 2020, 4, 2000238.	4.6	22
350	Novel (Ni, Fe)S2/(Ni, Fe)3S4 solid solution hybrid: an efficient electrocatalyst with robust oxygen-evolving performance. Science China Chemistry, 2020, 63, 1030-1039.	4.2	22
351	Ultrahigh Performance Triboelectric Nanogenerator Enabled by Charge Transmission in Interfacial Lubrication and Potential Decentralization Design. Research, 2022, 2022, .	2.8	22
352	Novel Gas-Induced-Reduction Route to Chalcogenide Nanostructures Taking Sb2Se3as an Example. Crystal Growth and Design, 2011, 11, 4759-4767.	1.4	21
353	Flexible quantum dot-sensitized solar cells with improved efficiencies based on woven titanium wires. Journal of Materials Chemistry A, 2014, 2, 15546.	5.2	21
354	Cellular internalization of LiNbO <sub>3</sub> nanocrystals for second harmonic imaging and the effects on stem cell differentiation. Nanoscale, 2016, 8, 7416-7422.	2.8	21
355	Hierarchical TiO <sub>2</sub> nanonetwork–porous Ti 3D hybrid photocatalysts for continuous-flow photoelectrodegradation of organic pollutants. Catalysis Science and Technology, 2017, 7, 524-532.	2.1	21
356	A method to visually observe the degradation-diffusion-reconstruction behavior of hydroxyapatite in the bone repair process. Acta Biomaterialia, 2020, 101, 554-564.	4.1	21
357	Homogeneous Chitosan/Graphene Oxide Nanocomposite Hydrogel-Based Actuator Driven by Efficient Photothermally Induced Water Gradients. ACS Applied Nano Materials, 2020, 3, 1002-1009.	2.4	21
358	Hydroxyapatite Nanorods Function as Safe and Effective Growth Factors Regulating Neural Differentiation and Neuron Development. Advanced Materials, 2021, 33, e2100895.	11.1	21
359	Piezotronic effect determined neuron-like differentiation of adult stem cells driven by ultrasound. Nano Energy, 2021, 90, 106634.	8.2	21
360	Size-Dependent Selective Etching Mechanism: Cavity Formation on Barium Titanate Nanocubes. Journal of Physical Chemistry C, 2008, 112, 17171-17174.	1.5	20

#	Article	IF	CITATIONS
361	Electrocatalytic oxidation of nucleobases by TiO2 nanobelts. Physical Chemistry Chemical Physics, 2011, 13, 9232.	1.3	20
362	Charge Transport at the Metal-Organic Interface. Annual Review of Physical Chemistry, 2013, 64, 221-245.	4.8	20
363	Periodically poled self-frequency-doubling green laser fabricated from Nd:Mg:LiNbO_3 single crystal. Optics Express, 2015, 23, 17727.	1.7	20
364	Piezoelectric Microchip for Cell Lysis through Cell–Microparticle Collision within a Microdroplet Driven by Surface Acoustic Wave Oscillation. Small, 2019, 15, e1804593.	5.2	20
365	Fabrication of a uniform Au nanodot array/monolayer graphene hybrid structure for high-performance surface-enhanced Raman spectroscopy. Journal of Materials Science, 2020, 55, 591-602.	1.7	20
366	Nanotextured silk fibroin/hydroxyapatite biomimetic bilayer tough structure regulated osteogenic/chondrogenic differentiation of mesenchymal stem cells for osteochondral repair. Cell Proliferation, 2020, 53, e12917.	2.4	20
367	Role of carrier-transfer in the optical nonlinearity of graphene/Bi <sub>2</sub> Te <sub>3</sub> heterojunctions. Nanoscale, 2020, 12, 16956-16966.	2.8	20
368	Self-supporting Co0.85Se nanosheets anchored on Co plate as highly efficient electrocatalyst for hydrogen evolution reaction in both acidic and alkaline media. Nano Research, 2020, 13, 2950-2957.	5.8	20
369	Real-Time Tracking of Emitter Generation in a Zero-Dimensional Perovskite. Chemistry of Materials, 2021, 33, 3721-3728.	3.2	20
370	Stemness Maintenance and Massproduction of Neural Stem Cells on Poly L‣actic Acid Nanofibrous Membrane Based on Piezoelectriceffect. Small, 2022, 18, e2107236.	5.2	20
371	Formation mechanism of black LiTaO <sub>3</sub> single crystals through chemical reduction. Journal of Applied Crystallography, 2011, 44, 158-162.	1.9	19
372	A Bi <sub>2</sub> WO <sub>6</sub> â€Based Hybrid Photocatalyst with Broad Spectrum Photocatalytic Properties under UV, Visible, and Nearâ€infrared Irradiation (Adv. Mater. 36/2013). Advanced Materials, 2013, 25, 5074-5074.	11.1	19
373	Large-scale synthesis and photoluminescence of cobalt tungstate nanowires. Physical Review B, 2013, 87, .	1.1	19
374	Conjugation of methotrexate onto dedoped Fe3O4/PPy nanospheres to produce magnetic targeting drug with controlled drug release and targeting specificity for HeLa cells. Synthetic Metals, 2015, 207, 18-25.	2.1	19
375	Formation mechanism and elimination methods for anti-site defects in LiNbO3/LiTaO3 crystals. CrystEngComm, 2016, 18, 8136-8146.	1.3	19
376	Facile synthesis of hierarchical porous Ni <sub>x</sub> Co <sub>1â^'x</sub> SeO <sub>3</sub> networks with controllable composition as a new and efficient water oxidation catalyst. Nanoscale, 2019, 11, 3268-3274.	2.8	19
377	Manipulating all-pH hydrogen evolution kinetics on metal sulfides through one-pot simultaneously derived multi-interface engineering and phosphorus doping. Journal of Materials Chemistry A, 2021, 9, 25539-25546.	5.2	19
378	Regulation of Neural Differentiation of ADMSCs using Grapheneâ€Mediated Wireless‣ocalized Electrical Signals Driven by Electromagnetic Induction. Advanced Science, 2022, 9, e2104424.	5.6	19

#	Article	IF	CITATIONS
379	Etching silicon wafer without hydrofluoric acid. Applied Physics Letters, 2005, 87, 261913.	1.5	18
380	Influence of chemical reduction on optical and electrical properties of LiTaO3 crystal. Journal of Alloys and Compounds, 2010, 497, 412-415.	2.8	18
381	Charge transport at the metal oxide and organic interface. Nanoscale, 2012, 4, 7301.	2.8	18
382	Introducing kalium into copper sulfide for the enhancement of thermoelectric properties. Journal of Materials Chemistry A, 2013, 1, 13721.	5.2	18
383	Effects of hydroxyapatite nanostructure on channel surface of porcine acellular dermal matrix scaffold on cell viability and osteogenic differentiation of human periodontal ligament stem cells. International Journal of Nanomedicine, 2013, 8, 1887.	3.3	18
384	Pseudo-Janus Zn/Al-based nanocomposites for Cr(VI) sorption/remediation and evolved photocatalytic functionality. Chemical Engineering Journal, 2015, 277, 150-158.	6.6	18
385	High Performance Supercapacitors from Hierarchical Porous Carbon Aerogels Based on Sliced Bread. Chinese Journal of Chemistry, 2017, 35, 699-706.	2.6	18
386	Nanocelluloseâ€Reinforced Hydroxyapatite Nanobelt Membrane as a Stem Cell Multiâ€Lineage Differentiation Platform for Biomimetic Construction of Bioactive 3D Osteoid Tissue In Vitro. Advanced Healthcare Materials, 2021, 10, e2001851.	3.9	18
387	Optical waveguide in stoichiometric lithium niobate formed by 500 keV proton implantation. Optics Express, 2007, 15, 16880.	1.7	17
388	A Novel Cold-Adapted Lipase from Sorangium cellulosum Strain So0157-2: Gene Cloning, Expression, and Enzymatic Characterization. International Journal of Molecular Sciences, 2011, 12, 6765-6780.	1.8	17
389	Surfactantless photochemical growth of Ag nanostructures on GaN epitaxial films with controlled morphologies and their application for SERS. Journal of Materials Chemistry, 2012, 22, 2410-2418.	6.7	17
390	Synthesis and biological evaluation of 2-amino-5-aryl-3-benzylthiopyridine scaffold based potent c-Met inhibitors. Bioorganic and Medicinal Chemistry, 2013, 21, 6804-6820.	1.4	17
391	Thermally-assisted photodegradation of lignin by TiO2/H2O2 under visible/near-infrared light irradiation. Science China Materials, 2018, 61, 382-390.	3.5	17
392	Dielectric and piezoelectric properties of lanthanum-modified 0.55Pb(Sc1/2Ta1/2)O3–0.45PbTiO3 ceramics. Journal of the European Ceramic Society, 2000, 20, 2337-2346.	2.8	16
393	Fabrication of 3D Pt catalysts via support of Na2Ti3O7 nanowires for methanol and ethanol electrooxidation. Catalysis Communications, 2010, 12, 100-104.	1.6	16
394	Quantitative Imaging of Single Unstained Magnetotactic Bacteria by Coherent X-ray Diffraction Microscopy. Analytical Chemistry, 2015, 87, 5849-5853.	3.2	16
395	Yb Sensitized Near-Stoichiometric Er:LiNbO3 Single Crystal: A Matrix for Optical Communication and Upconversion Emission. Crystal Growth and Design, 2018, 18, 1495-1500.	1.4	16
396	Two-photon fluorescent polydopamine nanodots for CAR-T cell function verification and tumor cell/tissue detection. Journal of Materials Chemistry B, 2018, 6, 6459-6467.	2.9	16

#	Article	IF	CITATIONS
397	Endowing Polyetheretherketone Implants with Osseointegration Properties: In Situ Construction of Patterned Nanorod Arrays. Small, 2022, 18, e2105589.	5.2	16
398	Synergistic coupling of NiFeZn-OH nanosheet network arrays on a hierarchical porous NiZn/Ni heterostructure for highly efficient water splitting. Science China Materials, 2022, 65, 1207-1216.	3.5	16
399	Adaptation of Salt-tolerant Myxococcus Strains and their Motility Systems to the Ocean Conditions. Microbial Ecology, 2007, 54, 43-51.	1.4	15
400	Enhancement of passively Q-switched performance at 134 $\hat{l}^{1}/4m$ with a class of Nd:GdxY_1-xVO_4 crystals. Optics Express, 2010, 18, 21551.	1.7	15
401	Preparation of WO3 network squares for ultrasensitive photodetectors. Journal of Alloys and Compounds, 2011, 509, L255-L261.	2.8	15
402	X-ray and neutron diffraction studies of flux and hydrothermally grown nonlinear optical material KBe2BO3F2. CrystEngComm, 2012, 14, 6079.	1.3	15
403	Al <sub>2</sub> O <sub>3</sub> /yttrium compound core–shell structure formation with burst nucleation: a process driven by electrostatic attraction and high surface energy. RSC Advances, 2014, 4, 55400-55406.	1.7	15
404	Cytocompatible 3D chitosan/hydroxyapatite composites endowed with antibacterial properties: toward a self-sterilized bone tissue engineering scaffold. Science Bulletin, 2015, 60, 1193-1202.	4.3	15
405	Synthesis and characterization of lithium niobium borate glasses containing neodymium. Journal of Rare Earths, 2016, 34, 1199-1205.	2.5	15
406	Top-seeded growth of K2Al2B2O7. Journal of Crystal Growth, 2001, 231, 439-441.	0.7	14
407	Seawater-Regulated Genes for Two-Component Systems and Outer Membrane Proteins in <i>Myxococcus</i> . Journal of Bacteriology, 2009, 191, 2102-2111.	1.0	14
408	Pt Nanoparticles Supported Inside TiO <sub>2</sub> Nanotubes for Effective Ethanol Electrooxidation. Journal of the Electrochemical Society, 2013, 160, H793-H799.	1.3	14
409	Mechanism of ammonium sulfate regulation effect on microstructure of Y2O3 nanopowders via urea precipitation method. CrystEngComm, 2013, 15, 5076.	1.3	14
410	Effect of composition deviation on the microstructure and luminescence properties of Nd:YAG ceramics. CrystEngComm, 2014, 16, 10856-10862.	1.3	14
411	Biodegradable inorganic nanoparticles: an opportunity for improved cancer therapy?. Nanomedicine, 2017, 12, 959-961.	1.7	14
412	Effect of Hydroxyapatite Nanorods on the Fate of Human Adiposeâ€Derived Stem Cells Assessed In Situ at the Single Cell Level with a Highâ€Throughput, Realâ€Time Microfluidic Chip. Small, 2019, 15, e1905001.	5.2	14
413	Synthesis and characterization of a coaxial carbon-TiO2 nanotube arrays film with spectral response from UV to NIR and its application in solar energy conversion. Electrochimica Acta, 2019, 301, 325-331.	2.6	14
414	Construction of High Stable Allâ€Grapheneâ€Based FETs as Highly Sensitive Dualâ€&ignal miRNA Sensors by a Covalent Layerâ€byâ€Layer Assembling Method. Advanced Electronic Materials, 2020, 6, 2000731.	2.6	14

#	Article	IF	CITATIONS
415	A wafer-scale two-dimensional platinum monosulfide ultrathin film via metal sulfurization for high performance photoelectronics. Materials Advances, 2022, 3, 1497-1505.	2.6	14
416	Growth and optical properties of ErCa4O(BO3)3 crystals. Journal of Crystal Growth, 2002, 234, 699-703.	0.7	13
417	Glassy State Lead Tellurite Nanobelts: Synthesis and Properties. Nanoscale Research Letters, 2010, 5, 1344-1350.	3.1	13
418	Enhancement of selective determination of the perfect match and mismatch of single nucleobases with a biosensing electrode based on surface-coarsened anatase TiO2 nanobelts. Journal of Materials Chemistry, 2011, 21, 10633.	6.7	13
419	Nano-p–n junction heterostructure TiO2 nanobelts for the electrochemical detection of anticancer drug and biointeractions with cancer cells. Journal of Materials Chemistry B, 2013, 1, 2072.	2.9	13
420	A novel stearate melting method for synthesizing highly reactive YAG nanopowders. Journal of Alloys and Compounds, 2014, 585, 48-53.	2.8	13
421	Specific detection of potassium ion in serum by a modified G-quadruplex method. RSC Advances, 2016, 6, 41999-42007.	1.7	13
422	Surface-sulfurized Ag2O nanoparticles with stable full-solar-spectrum photocatalytic activity. Chinese Journal of Catalysis, 2017, 38, 1063-1071.	6.9	13
423	Reduction of the ambient effect in multilayer InSe transistors and a strategy toward stable 2D-based optoelectronic applications. Nanoscale, 2020, 12, 18356-18362.	2.8	13
424	Self-reduction derived nickel nanoparticles in CdS/Ni(OH)2 heterostructure for enhanced photocatalytic hydrogen evolution. Journal of Chemical Physics, 2020, 152, 214701.	1.2	13
425	Controllable Nanoparticle Aggregation through a Superhydrophobic Laser-Induced Graphene Dynamic System for Surface-Enhanced Raman Scattering Detection. ACS Applied Materials & Interfaces, 2022, 14, 3504-3514.	4.0	13
426	Ag@CeO <sub>2</sub> –Au Nanorod Plasmonic Nanohybrids for Enhanced Photocatalytic Conversion of Benzyl Alcohol to Benzaldehyde. ACS Applied Nano Materials, 2022, 5, 4972-4982.	2.4	13
427	Highly specific differentiation of MSCs into neurons directed by local electrical stimuli triggered wirelessly by electromagnetic induction nanogenerator. Nano Energy, 2022, 100, 107483.	8.2	13
428	New Locus Important for <i>Myxococcus</i> Social Motility and Development. Journal of Bacteriology, 2007, 189, 7937-7941.	1.0	12
429	Construction of strong alkaline hydrothermal environment for synthesis of copper telluride nanowires. Solid State Sciences, 2011, 13, 1858-1864.	1.5	12
430	Enhancement of photocatalytic properties of TiO2 nanobelts through surface-coarsening and surface nanoheterostructure construction. Materials Science and Engineering B: Solid-State Materials for Advanced Technology, 2011, 176, 921-925.	1.7	12
431	Aligned open-ended carbon nanotube membranes for direct electrochemistry applications. Sensors and Actuators B: Chemical, 2012, 174, 570-576.	4.0	12
432	Nd:MgO:LiTaO3 crystal for self-doubling laser applications: growth, structure, thermal and laser properties. CrystEngComm, 2013, 15, 7468.	1.3	12

#	Article	IF	CITATIONS
433	Growth, structural, optical and thermal properties of Yb-doped and Yb–Mg codoped LiNbO3 single crystals. Journal of Alloys and Compounds, 2013, 564, 1-7.	2.8	12
434	Synthesis process and photocatalytic properties of BiOBr nanosheets for gaseous benzene. Environmental Science and Pollution Research, 2016, 23, 17525-17531.	2.7	12
435	Preparation of Ag2O/TiO2/fly-ash cenospheres composite photocatalyst. Materials Letters, 2016, 183, 444-447.	1.3	12
436	Upconversion single-photon detectors based on integrated periodically poled lithium niobate waveguides [Invited]. Journal of the Optical Society of America B: Optical Physics, 2018, 35, 2096.	0.9	12
437	Hybrid nanostructures of pit-rich TiO <sub>2</sub> nanocrystals with Ru loading and N doping for enhanced solar water splitting. Chemical Communications, 2019, 55, 2781-2784.	2.2	12
438	Spatiotemporal Oscillation in Confined Epithelial Motion upon Fluid-to-Solid Transition. ACS Nano, 2021, 15, 7618-7627.	7.3	12
439	Surface specifically modified NK-92 cells with CD56 antibody conjugated superparamagnetic Fe <sub>3</sub> O <sub>4</sub> nanoparticles for magnetic targeting immunotherapy of solid tumors. Nanoscale, 2021, 13, 19109-19122.	2.8	12
440	Stem Cell Membraneâ€Encapsulated Zeolitic Imidazolate Frameworkâ€8: A Targeted Nanoâ€Platform for Osteogenic Differentiation. Small, 2022, 18, .	5.2	12
441	A Photocatalytic Reduction Method for the Preparation of TiO <sub>2</sub> Nanobelt Supported Noble Metals (Ag, Au). Journal of Nanoscience and Nanotechnology, 2009, 9, 2119-2123.	0.9	11
442	Synthesis of stoichiometric LiNbO <sub>3</sub> nanopowder through a wet chemical method. Crystal Research and Technology, 2009, 44, 1235-1240.	0.6	11
443	Hydrothermal and wet-chemical synthesis of pure LiTaO3 powders by using commercial tantalum hydroxide as starting material. Journal of Alloys and Compounds, 2009, 477, 688-691.	2.8	11
444	In situ synthesis of TiH2 layer on metallic titanium foil through gaseous hydrogen free acid-hydrothermal method. Materials Research Bulletin, 2014, 50, 379-384.	2.7	11
445	Synthesis and characterization of translucent MgO-doped Al2O3 hollow spheres in millimeter-scale. Journal of Alloys and Compounds, 2014, 608, 185-190.	2.8	11
446	Effects of Carbon Pre-Germanidation Implantation on the Thermal Stability of NiGe and Dopant Segregation on Both n- and p-Type Ge Substrate. ECS Journal of Solid State Science and Technology, 2015, 4, P119-P123.	0.9	11
447	Localized committed differentiation of neural stem cells based on the topographical regulation effects of TiO <sub>2</sub> nanostructured ceramics. Nanoscale, 2016, 8, 13186-13191.	2.8	11
448	Photocatalytic quartz fiber felts with carbon-connected TiO2 nanoparticles for capillarity-driven continuous-flow water treatment. Applied Physics A: Materials Science and Processing, 2018, 124, 1.	1.1	11
449	The Porous Wafer of Pt Nanoparticle/TiO <sub>2</sub> Nanobelt Heterostructures with Enhanced Photocatalytic Activity Assisted with Catalytic Reaction of Pt. Science of Advanced Materials, 2014, 6, 538-544.	0.1	11
450	Gold Nanostrip Arrayâ€Mediated Wireless Electrical Stimulation for Accelerating Functional Neuronal Differentiation. Advanced Science, 2022, 9, .	5.6	11

#	Article	IF	CITATIONS
451	Antibiotic glass slide coated with silver nanoparticles and its antimicrobial capabilities. Polymers for Advanced Technologies, 2008, 19, 1455-1460.	1.6	10
452	Microstructural characteristics of Nd:YAG powders leading to transparent ceramics. Journal of Rare Earths, 2011, 29, 585-591.	2.5	10
453	Structure and resistivity of bismuth nanobelts in situ synthesized on silicon wafer through an ethanol-thermal method. Journal of Solid State Chemistry, 2011, 184, 3257-3261.	1.4	10
454	Alkali titanate nanobelts-supported Pd catalysts for room temperature formaldehyde oxidation. Catalysis Communications, 2020, 142, 106034.	1.6	10
455	Efficient Photocatalytic Degradation of RhB by Constructing Sn3O4 Nanoflakes on Sulfur-Doped NaTaO3 Nanocubes. Crystals, 2021, 11, 59.	1.0	10
456	Steering spatially separated dual sites on nano-TiO2 through SMSI and lattice matching for robust photocatalytic hydrogen evolution. Chinese Chemical Letters, 2021, 32, 3613-3618.	4.8	10
457	Biomaterial Cues Regulated Differentiation of Neural Stem Cells into GABAergic Neurons through Ca <sup>2+</sup> /c-Jun/TLX3 Signaling Promoted by Hydroxyapatite Nanorods. Nano Letters, 2021, 21, 7371-7378.	4.5	10
458	Large area uniform PtSx synthesis on sapphire substrate for performance improved photodetectors. Applied Materials Today, 2021, 25, 101176.	2.3	10
459	Growth of NaFe4P12Skutterudite Single Crystalline Nanosprings Synthesized through a Hydrothermalâ^'Reductionâ^'Alloying Method. Journal of Physical Chemistry B, 2004, 108, 13254-13257.	1.2	9
460	Cloning and characterization of an rRNA methyltransferase from Sorangium cellulosum. Biochemical and Biophysical Research Communications, 2008, 370, 140-144.	1.0	9
461	Growth of PbTe nanorods controlled by polymerized tellurium anions and metal(II) amides via composite-hydroxide-mediated approach. Materials Research Bulletin, 2009, 44, 1846-1849.	2.7	9
462	Preparation and Characterizations of Na <sub>2</sub> Ti <sub>3</sub> O <sub>7</sub> , H <sub>2</sub> Ti <sub>3</sub> O <sub>7</sub> and TiO <sub>2</sub> Nanobelts. Advanced Materials Research, 0, 306-307, 1233-1237.	0.3	9
463	Delaminated sodium titanate nanobelts in synergy with cationic polyacrylamide to induce flocculation on kaolin clay. Colloids and Surfaces A: Physicochemical and Engineering Aspects, 2012, 414, 9-16.	2.3	9
464	Diversity of epothilone producers among S orangium strains in producerâ€positive soil habitats. Microbial Biotechnology, 2014, 7, 130-141.	2.0	9
465	Nano-p–n junction heterostructures enhanced TiO2 nanobelts biosensing electrode. Journal of Solid State Electrochemistry, 2014, 18, 2693-2699.	1.2	9
466	KTP OPO with signal wave at 1630 nm intracavity pumped by an efficient σ-polarized Nd,MgO:LiNbO_3 laser. Optical Materials Express, 2015, 5, 684.	1.6	9
467	Static pressure-induced neural differentiation of mesenchymal stem cells. Nanoscale, 2017, 9, 10031-10037.	2.8	9
468	Rapamycin/sodium hyaluronate binding on nano-hydroxyapatite coated titanium surface improves MC3T3-E1 osteogenesis. PLoS ONE, 2017, 12, e0171693.	1.1	9

#	Article	IF	CITATIONS
469	Ultralow Saturation Intensity Topological Insulator Saturable Absorber for Gigahertz Mode-Locked Solid-State Lasers. IEEE Photonics Journal, 2018, 10, 1-10.	1.0	9
470	Compact all-fiber polarization-independent up-conversion single-photon detector. Optics Communications, 2019, 441, 185-189.	1.0	9
471	Neuron-like cell differentiation of hADSCs promoted by a copper sulfide nanostructure mediated plasmonic effect driven by near-infrared light. Nanoscale, 2020, 12, 9833-9841.	2.8	9
472	Cu <sub>2</sub> S/BiVO <sub>4</sub> Heterostructure Photoanode with Extended Wavelength Range for Efficient Water Splitting. Journal of Physical Chemistry C, 2021, 125, 15890-15898.	1.5	9
473	Ag Nanoparticles Anchored on Nanoporous Ge Skeleton as <scp>Highâ€Performance</scp> Anode for Lithiumâ€ion Batteries. Chinese Journal of Chemistry, 2021, 39, 2881-2888.	2.6	9
474	Synthesis and Visible Light Photo-Electrochemical Behavior of In <sub>2</sub> O <sub>3</sub> -Sensitized TiO <sub>2</sub> Nanorod Arrays. Science of Advanced Materials, 2013, 5, 796-802.	0.1	9
475	High-Performance Supercapacitors Based on Nitrogen-Doped Porous Carbon from Surplus Sludge. Science of Advanced Materials, 2015, 7, 571-578.	0.1	9
476	Spiral growth mechanisms of CMTD crystals. Journal of Crystal Growth, 2004, 261, 63-69.	0.7	8
477	Synthesis, Characterization, and Electrical Properties of SiCN Nanowires. Crystal Growth and Design, 2008, 8, 2144-2149.	1.4	8
478	Flux Growth and Characterizations of Ga3PO7 Single Crystals. Crystal Growth and Design, 2008, 8, 3577-3580.	1.4	8
479	Preparation and characterization of nanostructured Bi2Se3 and Sn0.5-Bi2Se3. Rare Metals, 2009, 28, 112-116.	3.6	8
480	Growth of MgO doped near stoichiometric LiNbO3 single crystals by a hanging crucible Czochralski method using a ship lockage type powder feeding system assisted by numerical simulation. CrystEngComm, 2014, 16, 6593.	1.3	8
481	Scaly Graphene Oxide/Graphite Fiber Hybrid Electrodes for DNA Biosensors. Advanced Materials Interfaces, 2015, 2, 1500072.	1.9	8
482	Preparation of In <sub>2</sub> S <sub>3</sub> @TiO <sub>2</sub> Nanobelt Heterostructures with High UV-Visible Light Photocatalytic Activities. Science of Advanced Materials, 2015, 7, 479-488.	0.1	8
483	Are graphene-Bi <sub>2</sub> Te <sub>3</sub> van der Waals heterostructure-based saturable absorbers promising for solid-state Q-switched lasers?. Optics Letters, 2019, 44, 1072.	1.7	8
484	Twin structure in Yb:YAl3(BO3)4crystal. Journal of Applied Crystallography, 2001, 34, 661-662.	1.9	7
485	Synthesis and characterization of KCu3S2 microstructures through a composite-hydroxide mediated method. Journal of Alloys and Compounds, 2010, 507, 429-432.	2.8	7

Dispersion of concentrated aqueous neodymiaâ  $\in$  "yttriaâ  $\in$ " alumina mixture with ammonium poly(acrylic) Tj ETQq0 0.0 rgBT /  $\mathcal{O}$  verlock 10  $\mathcal{O}$  ver

#	Article	IF	CITATIONS
487	Increasing the extraction efficiency of blue light emitting diodes via laser patterned Gaâ€polar pâ€GaN surface. Physica Status Solidi (A) Applications and Materials Science, 2011, 208, 2226-2230.	0.8	7
488	Ultrasonic irradiation assisted surface modification of titanium plates to improve MC3T3-E1 cell proliferation. Ultrasonics Sonochemistry, 2013, 20, 216-221.	3.8	7
489	Hierarchically Assembled ZnO Nanorods on TiO <sub>2</sub> Nanobelts for High Performance Gas Sensor. Energy and Environment Focus, 2014, 3, 404-410.	0.3	7
490	A general strategy to fabricate ligand-free water-soluble up-conversion nanoparticles. Journal of Alloys and Compounds, 2014, 613, 18-24.	2.8	7
491	Coordination ability determined transition metal ions substitution of Tb in Tb-Asp fluorescent nanocrystals and a facile ions-detection approach. Nanoscale, 2018, 10, 7526-7535.	2.8	7
492	Morphology-dependent highly active microcrystalline stannous oxalate photocatalysts with selectively exposed facets and low specific surface areas. Applied Surface Science, 2020, 525, 146347.	3.1	7
493	Topographical regulation of stem cell differentiation by plant-derived micro/nanostructures. Nanoscale, 2020, 12, 18305-18312.	2.8	7
494	Unilateral Silver-Loaded Silk Fibroin Difunctional Membranes as Antibacterial Wound Dressings. ACS Omega, 2021, 6, 17555-17565.	1.6	7
495	Fast Charge Transportation and Enhanced Photocatalytic and Photo-Electrochemical Performance of 3D Hierarchical TiO <sub>2</sub> Nano-Whisker/Graphite Fiber Heterostructure. Science of Advanced Materials, 2015, 7, 319-328.	0.1	7
496	Growth and defects in YbxY1â^'xAl3(BO3)4 crystals. Journal of Crystal Growth, 2001, 229, 256-260.	0.7	6
497	Growth mechanism of single crystal NaFe4P12 nanowires. Journal of Crystal Growth, 2002, 234, 679-682.	0.7	6
498	Charge conversion and mass transfer on surface of Al2O3 nanoparticles in Y2O3–Al2O3 colloidal system. CrystEngComm, 2013, 15, 4335.	1.3	6
499	A general method for mass and template-free production of hierarchical metal oxide spheres at room-temperature. RSC Advances, 2014, 4, 24176-24182.	1.7	6
500	Antisite defect elimination through Mg doping in stoichiometric lithium tantalate powder synthesizedviaa wet-chemical spray-drying method. Journal of Applied Crystallography, 2015, 48, 377-385.	1.9	6
501	Effects of carbon pre-germanidation implant into Ge on the thermal stability of NiGe films. Microelectronic Engineering, 2015, 133, 6-10.	1.1	6
502	Ferromagnetism in chemically reduced LiNbO <sub>3</sub> and LiTaO <sub>3</sub> crystals. Journal Physics D: Applied Physics, 2016, 49, 195005.	1.3	6
503	Synthesis of AgCl/Ag/AgCl core-shell microstructures with enhanced photocatalytic activity under sunlight irradiation. Journal of Environmental Chemical Engineering, 2016, 4, 4021-4028.	3.3	6
504	De-escalation empirical antibiotic therapy improved survival for patients with severe aplastic anemia treated with antithymocyte globulin. Medicine (United States), 2017, 96, e5905.	0.4	6

#	Article	IF	CITATIONS
505	Nanostructured titanium foam with metal ions incorporation for promoting osteogenic differentiation of mesenchymal stem cells. Journal of Alloys and Compounds, 2017, 729, 816-822.	2.8	6
506	An In Situ Polymerizationâ€Encapsulation Approach to Prepare TiO <sub>2</sub> –Graphite Carbon–Au Photocatalysts for Efficient Photocatalysis. Particle and Particle Systems Characterization, 2018, 35, 1700297.	1.2	6
507	Bio-inspired synthesis of mesoporous HfO2 nanoframes as reactors for piezotronic polymerization and Suzuki coupling reactions. Nanoscale, 2019, 11, 5240-5246.	2.8	6
508	A Facile and Sensitive DNA Sensing of Harmful Algal Blooms Based on Graphene Oxide Nanosheets. Marine Biotechnology, 2020, 22, 498-510.	1.1	6
509	Growth of large size near-stoichiometric lithium niobate single crystals with low coercive field for manufacturing high quality periodically poled lithium niobate. Optical Materials, 2022, 125, 112058.	1.7	6
510	Triangular dendrites of LiAlSiO4–SiO2: evolution between threefold- and sixfold-symmetric morphologies. Journal of Applied Crystallography, 2002, 35, 455-458.	1.9	5
511	Electrokinetic properties of Nd:YAG nanopowder and a high concentration slurry with ammonium poly(acrylic acid) as dispersant. Journal of Materials Science, 2010, 45, 706-712.	1.7	5
512	Three-wavelength green laser using intracavity frequency conversion of Nd:Mg:LiTaO3 with a MgO:PPLN crystal. Applied Physics B: Lasers and Optics, 2014, 117, 1117-1121.	1.1	5
513	Experimental and theoretical investigation on passively Q-switched laser action in c-cut Nd:MgO:LiNbO_3. Applied Optics, 2015, 54, 9354.	2.1	5
514	Multi-spectral and thermodynamic analysis of the interaction mechanism between Cu2+ and α-amylase and impact on sludge hydrolysis. Environmental Science and Pollution Research, 2017, 24, 9428-9436.	2.7	5
515	3D hierarchical macro/mesoporous TiO <sub>2</sub> with nanoporous or nanotubular structures and their core/shell composites achieved by anodization. CrystEngComm, 2017, 19, 2509-2516.	1.3	5
516	Co Nanoparticles@N-doped carbon coated on carbon Nanotube@Defective silica as non-noble photocathode for efficient photoelectrochemical hydrogen generation. International Journal of Hydrogen Energy, 2018, 43, 9279-9286.	3.8	5
517	Facile approach for the periodic poling of MgO-doped lithium niobate with liquid electrodes. CrystEngComm, 2019, 21, 941-947.	1.3	5
518	Cobalt Oxide Modified Highly Ordered TiO <sub>2</sub> Nanotube Arrays: Enhanced Visible Light Photoelectrochemical Properties. Science of Advanced Materials, 2013, 5, 1256-1263.	0.1	5
519	A Living Material Constructed from Stem Cells for Tumorâ€Tropic Oncotherapy with Realâ€Time Imaging. Advanced Functional Materials, 2022, 32, .	7.8	5
520	Image shifts resulting from the misorientation of two individuals in GdCa4O(BO3)3 crystal. Journal of Crystal Growth, 2001, 229, 252-255.	0.7	4
521	Growth and thermal properties of LaCa4O(BO3)3 crystals. Optical Materials, 2003, 23, 461-464.	1.7	4
522	Electrical and photoluminescent behaviors of La(OH)3 nanobelts doped with Ce3+ and Er3+. Materials Chemistry and Physics, 2010, 123, 502-506.	2.0	4

#	Article	IF	CITATIONS
523	CdS thin films on LiNbO3 (104) and silicon (111) substrates prepared through an atom substitution method. Journal of Solid State Chemistry, 2011, 184, 725-728.	1.4	4
524	Spin coating-Co-reduction approach: A general strategy for preparation of oriented chalcogenide thin film on arbitrary substrates. Rare Metals, 2011, 30, 651-656.	3.6	4
525	Optimization of a two-step Ni(5% Pt) germanosilicidation process and the redistribution of Pt in Ni(Pt)Si1â^'Ge germanosilicide. Vacuum, 2015, 111, 114-118.	1.6	4
526	Self-templated synthesis of TiO2 hierarchical structure photocatalyst with high efficiency and good sedimentation property. Applied Physics A: Materials Science and Processing, 2016, 122, 1.	1.1	4
527	Exploring the Effect of Cu2+ on Sludge Hydrolysis and Interaction Mechanism between Cu2+ and Xylanase by Multispectral and Thermodynamic Methods. Water, Air, and Soil Pollution, 2017, 228, 1.	1.1	4
528	Origin of Ferroelectric Modification: The Thermal Behavior of Dopant Ions. Crystal Growth and Design, 2018, 18, 4860-4863.	1.4	4
529	HAp Thermosensitive Nanohydrogel Cavities Act as Brood Pouches to Incubate and Controlâ€Release NSCs for Rapid Spinal Cord Injury Therapy. Advanced Functional Materials, 0, , 2203492.	7.8	4
530	Lowâ€dose ion implanted active waveguides in Nd <sup>3+</sup> doped nearâ€stoichiometric lithium niobate: promising candidates for near infrared integrated laser. Physica Status Solidi - Rapid Research Letters, 2008, 2, 141-143.	1.2	3
531	Twinning structures in near-stoichiometric lithium niobate single crystals. Journal of Applied Crystallography, 2010, 43, 276-279.	1.9	3
532	(111) Twinned BaTiO3 microcrystallites. CrystEngComm, 2010, 12, 3003.	1.3	3
533	Fabrication and laser output of transparent Nd:YAG ceramics from microwave synthesized precursors. Rare Metals, 2011, 30, 607-615.	3.6	3
534	An Impedimetricâ€Fluorescence Doubleâ€Checking Biosensor with Enhanced Reliability Based on Graphene Oxide. Advanced Materials Interfaces, 2015, 2, 1500279.	1.9	3
535	Cancer Therapy: Multifunctional Carbon-Silica Nanocapsules with Gold Core for Synergistic Photothermal and Chemo-Cancer Therapy under the Guidance of Bimodal Imaging (Adv. Funct. Mater.) Tj ETQq1	1 Ø. <b>ø</b> 8431	l4 <b>3</b> gBT /Ov∈
536	IDENTIFICATION OF ABNORMAL PHASE AND ITS FORMATION MECHANISM IN SYNTHESIZING CHALCOGENIDE FILMS. Surface Review and Letters, 2016, 23, 1550081.	0.5	3
537	Temperature dependent domain-wall moving dynamics of lithium niobate during high electric field periodic poling. Journal of Applied Physics, 2020, 128, 224101.	1.1	3
538	Electrochemical Insertion of Zinc Ions into Selfâ€Organized Titanium Dioxide Nanotube Arrays to Achieve Strong Osseointegration with Titanium Implants. Advanced Materials Interfaces, 2022, 9, .	1.9	3
539	Evolution of optical nonlinearity within graphene/Bi <sub>2</sub> Te <sub>3</sub> heterostructure. Journal of Materials Chemistry C, 0, , .	2.7	3
540	Ferroelectric Domain Reversal Dynamics in LiNbO <sub>3</sub> Optical Superlattice Investigated with a Realâ€īime Monitoring System. Small, 2022, 18, .	5.2	3

#	Article	IF	CITATIONS
541	Polycrystalline LaFe3CoSb12 material manufactured by melt-freeze-annealing method. Progress in Crystal Growth and Characterization of Materials, 2000, 40, 285-291.	1.8	2
542	Spectral properties of Nd-doped BiB3O6 crystal. Science in China Series B: Chemistry, 2001, 44, 510-515.	0.8	2
543	Research on crystal growth and properties of a new nonlinear optical crystal: Bismuth borate BiB3O6. Science Bulletin, 2001, 46, 1783-1785.	1.7	2
544	Bismuth onion thin film in situ grown on silicon wafer synthesized through a hydrothermal approach. Applied Surface Science, 2010, 257, 102-108.	3.1	2
545	2-Amino-3-nitropyridinium 4-hydroxybenzenesulfonate. Acta Crystallographica Section E: Structure Reports Online, 2012, 68, o2169-o2169.	0.2	2
546	Cell Lysis: Piezoelectric Microchip for Cell Lysis through Cell-Microparticle Collision within a Microdroplet Driven by Surface Acoustic Wave Oscillation (Small 9/2019). Small, 2019, 15, 1970050.	5.2	2
547	Morphology Tuned BaTiO3 Ceramic Sintering: Crystal Facet and Size Distribution. Science of Advanced Materials, 2016, 8, 1200-1207.	0.1	2
548	Progress in skutterudite-based thermoelectric materials. , 0, , .		1
549	GROWTH AND MELTING OF THE CLEAVAGE FACE \${10 ar{1}1}\$ of Yb:YAl3(BO3)4 Crystal. Surface Review and Letters, 2002, 09, 1395-1400.	0.5	1
550	Nano-dendrites in NaFe4P12 nano-wires synthesized by hydrothermal method. Optical Materials, 2003, 23, 475-478.	1.7	1
551	A Dendrite with "Sierpinski Gasket" Fractal Morphology in Matt Glaze of LiAlSiO4-SiO2 System. Fractals, 2003, 11, 271-276.	1.8	1
552	A Novel Mixed Hydroxide Method for Hydroxyapatite Preparation. Advanced Materials Research, 0, 152-153, 1399-1403.	0.3	1
553	LOW TEMPERATURE NEUTRON DIFFRACTION ON CONGRUENT AND NEAR STOICHIOMETRIC LiNbO3. Modern Physics Letters B, 2012, 26, 1250142.	1.0	1
554	Enhancement of Electrochemical Differentiation Ability of Nucleobases in Phosphate Buffer Solution at pH 7.4. Nucleosides, Nucleotides and Nucleic Acids, 2013, 32, 464-476.	0.4	1
555	The Phase and Morphology of Cu <sub><b>2</b></sub> ZnSnSe <sub><b>4</b></sub> Nanopowders by Hydrothermal Method. Journal of Nanomaterials, 2014, 2014, 1-5.	1.5	1
556	Electrochemistry Behavior of Ag/TiO <sub>2</sub> Nanobelts and its Potential Applications on Mercapto Proteins Detection. Journal of Nano Research, 2015, 37, 85-91.	0.8	1
557	Hierarchical structures of self-assembled hybrid calcium carbonate: nucleation kinetic studies on biomineralization. CrystEngComm, 2015, 17, 5372-5376.	1.3	1
	Stem Cell Fate: Effect of Hydroxyapatite Nanorods on the Fate of Human Adinoseâ€Derived Stem Cells		-

Stem Cell Fate: Effect of Hydroxyapatite Nanorods on the Fate of Human Adiposeâ€Derived Stem Cells Assessed In Situ at the Single Cell Level with a Highâ€Throughput, Realâ€Time Microfluidic Chip (Small) Tj ETQq0 0502rgBT /Overlock 10

#	Article	IF	CITATIONS
559	Serendipity of a topological nontrivial band gap in the 2D borophene subunit lattice with broken mirror symmetry. Physical Chemistry Chemical Physics, 2019, 21, 22526-22530.	1.3	1
560	Performanceâ€Enhanced CsPbBr 3 /HfO 2 /Si Heterostructure Optoelectronics through the Tunneling Effect. Advanced Materials Interfaces, 2021, 8, 2100279.	1.9	1
561	Effects of Humidity, Temperature and Time on the Nd:YAG Nano-powders during the Aging Process. Wuji Cailiao Xuebao/Journal of Inorganic Materials, 2011, 26, 1273-1280.	0.6	1
562	Preparation and thermoelectric properties of polyaniline/NaFe/sub 4/P/sub 12/ composite. , 0, , .		0
563	Whiteâ€beam synchrotron topographic characterization of antiparallel 180° domains in MgO doped nearâ€stoichiometric LiNbO <sub>3</sub> . Physica Status Solidi (A) Applications and Materials Science, 2008, 205, 1144-1147.	0.8	0
564	High power Nd:YAG ceramic lasers: passive Q-switching and frequency doubling. , 2009, , .		0
565	Selective Binding of Nucleobases and its Electrochemical Behavior at Glassy Carbon Electrode in PBS at pH 7.4. Advanced Materials Research, 2011, 239-242, 328-333.	0.3	0
566	Nd:Y2O3 Powder Synthesized by Low Temperature Calcination for Fabricating Transparent Ceramics. Journal of Inorganic and Organometallic Polymers and Materials, 2011, 21, 962-965.	1.9	0
567	Effects of Enzymes Treatment on Structure and Properties of Acellular Dermal Matrix. Applied Mechanics and Materials, 2012, 268-270, 233-236.	0.2	0
568	<i>A Special Issue on</i> Heterostructured Semiconductor Nanophotocatalyst: Design, Synthesis, and Applications. Energy and Environment Focus, 2014, 3, 317-319.	0.3	0
569	The Phase and Morphology of CuInSe2 Film Prepared by One-Step electrodeposition. Medziagotyra, 2017, 23, .	0.1	0
570	Fieldâ€Effect Transistors: A Facile and Effective Method for Patching Sulfur Vacancies of WS <sub>2</sub> via Nitrogen Plasma Treatment (Small 36/2019). Small, 2019, 15, 1970195.	5.2	0
571	Outside Front Cover: Volume 2 Issue 2. SmartMat, 2021, 2, i.	6.4	0
572	Establishment of <i>Sorangium cellulosum</i> So0157-2 Proteome Database Using Optimized Two-dimensional Electrophoresis Protocol*. Progress in Biochemistry and Biophysics, 2012, 39, 86-94.	0.3	0
573	Anti-CD19 ARTEMISTM Therapy Drastically Reduces Cytokine Release without Compromising Efficacy Against Preclinical Lymphoma Models. Blood, 2016, 128, 3354-3354.	0.6	0
574	The realization of a topological insulator saturable absorber-based mode-locked solid state laser. , 2018, , .		0
575	Front Cover Image. InformaÄnÃ-Materiály, 2021, 3, .	8.5	0